A climatological analysis of downstream precipitation extremes associated with recurving North Atlantic tropical cyclones

Master's Thesis

Faculty of Science

University of Bern

presented by

Roman Pohorsky

2017

Supervisor:

Prof. Dr. Olivia Romppainen-Martius

Institute of Geography of the University of Bern and Oeschger Centre for Climate Change Research, University of Bern

Advisor:

Matthias Röthlisberger

Abstract

Recurving tropical cyclones (TCs) interacting with the midlatitude upper-level waveguide are known to amplify waves on the latter. Subsequent downstream propagation of amplified Rossby waves can cause high impact weather (HIW) events in remote regions. Although previous case studies have attributed HIW events to recurving tropical cyclones, no climatological evidence has yet been established. The presented master's thesis addresses this research gap for North Atlantic recurving tropical cyclones and HIW events over the greater European area.

The HIW response to North Atlantic TC recurvature is evaluated based on a time-lagged composites of precipitation extremes following TC - jet interactions. The surface coverage and magnitude of precipitation extremes are assessed at a systematic distance from the location of the interaction between a recurving tropical cyclone and the jet stream. In a second phase, the influence of the midlatitude flow configuration (during the interaction) on the precipitation extremes response is assessed. A k-means clustering algorithm based on potential vorticity fields is used to define four major types of flow situations.

A novel bootstrapping technique using analog flow situations with no tropical cyclone is applied to disentangle the influence of the interacting tropical cyclone on precipitation extremes from the natural evolution of the midlatitude flow.

The method is applied to 147 cases of North Atlantic tropical cyclones recurving below 45° N between 1979 and 2013 for daily precipitation extremes from the ERA-Interim dataset.

The presented results indicate that on average, a significant increase in precipitation extremes occurs between 30 and 72 hours after the interaction onset, with three out of four major configurations leading to a statistically significant increase in precipitation extremes over Europe. The response is however sensitive to the jet configuration at the moment of the interaction. Further, the different types of interaction exhibit significant variability in terms of location of precipitation extremes and time lag between the interaction onset and the peak in precipitation extremes.

Contents

Chapter 1

Introduction

1.1 Motivation

Tropical cyclones (TCs) are amongst the most damaging meteorological phenomena on Earth (*Emanuel*, 2003). However, despite their tropical origin, their effect on surface extreme weather is not restricted to the tropics and subtropics (*Jones et al.*, 2003). In the North Atlantic, 46% of tropical cyclones do not make landfall in subtropical latitudes, but instead, recurve northward towards higher latitudes (*Hart and Evans*, 2001). When a tropical cyclone reaches higher latitudes, the environmental conditions are no longer favorable for its sustainment and it undergoes extratropical transition (ET) (*Jones et al.*, 2003), a process of transformation into an extratropical cyclone. Although extratropical cyclones do not typical sustain the same strength as tropical cyclones, they cover a much larger area and can be associated with extreme weather along their track (*Jones et al.*, 2003). However, the impact of a recurving tropical cyclone is not strictly limited to its direct vicinity. Recent studies have fostered interest in the interaction between recurving tropical cyclones and the extratropical jet stream. The interaction between a recurving tropical cyclone and the midlatitude waveguide can lead to the amplification of a Rossby wave packet (*Riemer et al.*, 2008; *Harr and Dea*, 2009). These waves propagate downstream and can potentially cause high-impact weather (HIW) events far from the actual cyclone's location (*Pinto et al.*, 2001; *Grams et al.*, 2011; *Pantillon et al.*, 2015). At the same time, due to the complexity of the processes involved in these interactions

and TC-tracks forecasting issues, the predictability of the midlatitude flow is often reduced after such interactions. Hence, it remains yet uncertain how systematically TC - jet interactions are followed by HIW events (*Anwender et al.*, 2008; *Grams et al.*, 2015).

1.2 Notions on TC - jet interaction and wave development

1.2.1 Downstream amplification of the midlatitude flow

There is clear evidence that recurving tropical cyclones do not only impact on the weather in their direct vicinity, but also affect more remote regions, particularly downstream (e.g. *Jones et al.*, 2003; *Agusti-Panareda et al.*, 2004; *Cordeira and Bosart*, 2011). The downstream impact of recurving TCs is governed by Rossby wave dynamics (*Hoskins et al.*, 1985; *Riemer et al.*, 2008; *Quinting and Jones*, 2016). When recurving cyclones reach higher latitudes, they interact with the midlatitude waveguide, which contributes to the amplification of the flow and leads to downstream propagating large-amplitude Rossby wave packets (*Hakim*, 2003; *Riemer et al.*, 2008). This amplified flow pattern can in turn initiate high impact weather events (*Harr and Dea*, 2009; *Grams and Blumer*, 2015).
In an idealized numerical study, *Riemer et al.* (2008) present the chain of events following the interaction between a cyclone and a straight jet. A Helmholtz partitioning of the surrounding TC's wind field in non-divergent and irrotational components and a piecewise potential vorticity (PV) inversion allowed to explain the role of the TC's outflow in the amplification of a downstream ridge. Following *Wernli and Davies* (1997), once a tropical cyclone leaves the inner tropics, diabatic processes in its convective center involve PV increase below the heating maximum level and PV destruction above it. Hence, air parcels rising in the TC center, reach the upper-troposphere with typical values between 0 and 0.5 PVU[1] (Potential vorticity units: $1PVU \equiv 10^{-6} \cdot K \cdot m^2 \cdot kg \cdot s$) (*Grams et al.*, 2011). This low PV air is then advected horizontally by the TC's outflowing circulation[1,2].
During the first stage of the interaction, the divergent outflow of the tropical cyclone is responsible for negative PV advection that deforms the PV contours northward of the TC and strengthens the meridional PV gradient[2] (*Grams et al.*, 2011; *Archambault et al.*,

[1]Real world observation results
[2]Idealized studies results

2013). It results in an acceleration and northward deflection of the jet stream[1,2] (Figure 1.1).

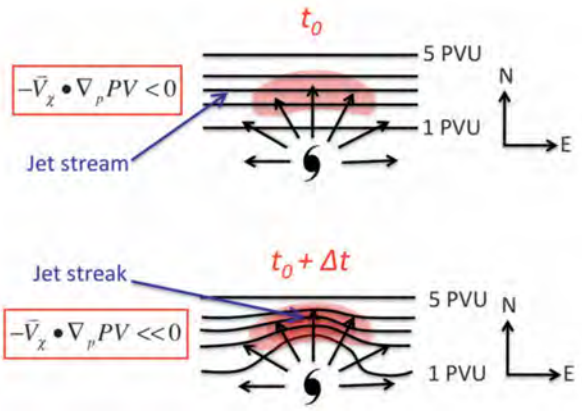

Figure 1.1: Idealized isentropic cross section of a TC - jet interaction from (*Archambault et al.*, 2013). Vectors represent the upper-level divergent outflow from the TC. Shading denotes the negative PV advection responsible for the jet acceleration and deflection. The equation represents the negative PV advection. A detailed explanation is given in section 2.2.1.

In a second phase, the outflow on the northeastern side of the cyclone contributes to the amplification of a downstream ridge[1] (*Jones et al.*, 2003; *Riemer et al.*, 2008; *Grams et al.*, 2011). The downstream ridge building and the intensifying curved jet streak (rapid jet stream) beget in turn, the elongation of a downstream trough[1,2] (*Archambault et al.*, 2013). Hence, the prominent features of the interaction of a tropical cyclone with the midlatitude waveguide are an amplified ridge-trough couplet and a distinct jet streak in the upper level flow. This upper-level ridge–trough pattern continues to propagate downstream as a wave and initiates a family of cyclones[2] (*Riemer et al.*, 2008). The further development of these waves is characterized by downstream baroclinic development[2] (*Orlanski and Sheldon*, 1995). The downstream effect of the ET system is usually seen most significantly one to two wavelengths downstream of the ET location[2] (*Riemer et al.*, 2008).

This scenario represents of course an ideal case. In a majority of cases, a recurving tropical cyclone does not interact with a straight jet, but a rather pre-amplified flow. *Riemer and Jones* (2010) reproduced a similar numerical experiment but assessed the impact of a recurving cyclone on a perturbed jet. They found that in the case of a recurving

[1]Real world observation results
[2]Idealized studies results

tropical cyclone interacting with a baroclinic wave, the TC's upper-level outflow was still responsible for a downstream ridge-trough couplet amplification that develops faster and is deeper than the control run with no interacting cyclone[2]. The amplitude of the resulting waves is, however, sensitive to the strength of the TC and its phasing with the initial baroclinic wave.

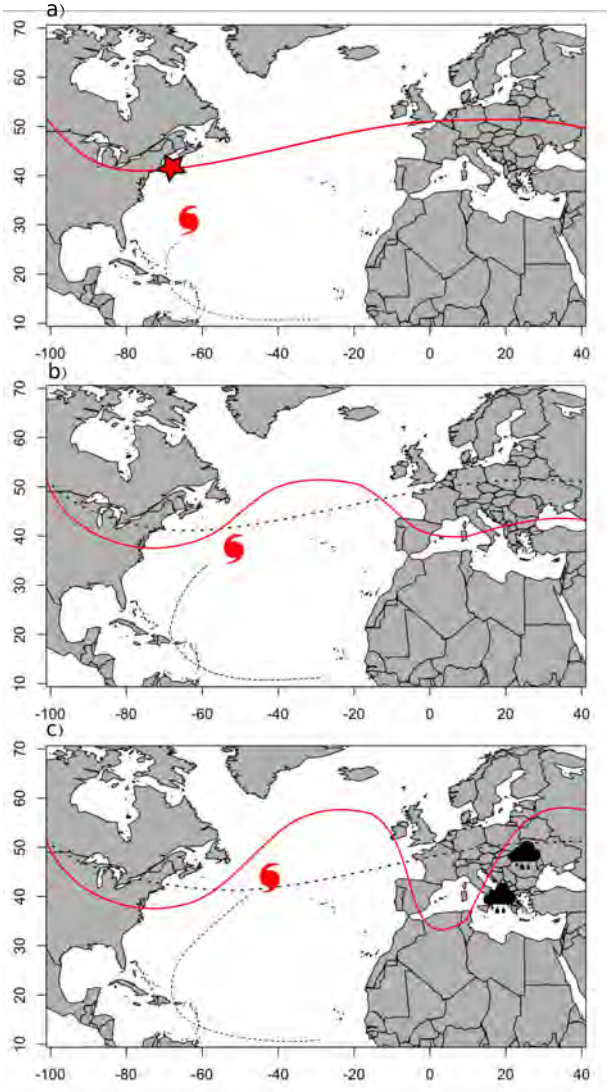

Figure 1.2: Idealized representation of the temporal evolution of Rossby waves' amplification following a recurving TC interacting with the jet stream. Panel (a) represents the interaction onset after recurvature. The red star represents the location of the strongest interaction. The red line represents the isentropic 2PVU line co-located with the extratropical jet stream. Panel (b) exhibits the amplification of a ridge located directly downstream of the TC. Panel (c) exhibits the further amplification of the ridge and the elongation of a trough downstream of the ridge. Heavy precipitation occurs on the eastern flank of the elongated trough.

[1]Real world observation results
[2]Idealized studies results

1.2.2 Importance of diabatic processes

Diabatic processes, occurring in the TC as well as in its surrounding, play a key role in the modification of the upper-level waveguide (e.g. *Massacand et al.*, 2001; *Agusti-Panareda et al.*, 2004; *Grams et al.*, 2011). Enhanced poleward moisture fluxes are associated with the recurving tropical cyclones. When this moist air reaches the midlatitude baroclinic region with upper-level forcing for ascent, diabatic processes occur and contribute to the modification of the upper-level Rossby wave pattern. *Grams and Archambault* (2016) have argued that conceptually, the extratropical transition of a recurving tropical cyclone is associated with 3 distinct weather systems. 1) A predecessor rain event, which precedes the recurving tropical cyclone. The cyclone's low-level circulation advects large plumes of moisture towards the midlatitude baroclinic zone. When this moist air is co-located with a region of upper-level forcing for ascent several days prior to the TC - jet interaction, heavy precipitation may occur as a result of quasi-stationary convection in that region. The strong latent heat release during the condensation of water vapor leads to an intense diabatic outflow. 2) The TC - extratropical jet interaction as already described in section 1.2.1. 3) Later, as the tropical cyclone gradually transforms into an extratropical cyclone, its central convection weakens. As the vertical convection gets reduced, the low-level circulation impinges on the midlatitude baroclinic zone and slantwise ascent establishes along a developing warm front. This maintains a low PV anomaly at upper-levels directly downstream of the cyclone (*Agusti-Panareda et al.*, 2004). Hence, the amplification process is maintained by a warm conveyor belt (WCB) like system.

These 3 systems exhibit strong diabatic outflows, which results in a transport of low PV air to the tropopause. This low PV air injection increases the horizontal PV gradient and favors downstream ridge building (*Grams and Archambault*, 2016).

1.2.3 High impact weather events

Since the link between TC - jet interactions and an amplified extratropical flow has been established, the attention has been drawn to the possible development of high impact weather events downstream (e.g. *Harr and Dea*, 2009; *Cordeira and Bosart*, 2011; *Grams and Blumer*, 2015; *Pantillon et al.*, 2015). The downstream dispersion of Rossby wave

packets (RWP) can in fact cause high impact weather events such as explosive surface cyclogenesis (*Agusti-Panareda et al.*, 2004; *Pantillon et al.*, 2015), cold air outbreaks (*Archambault et al.*, 2013) or severe precipitation associated to PV streamers (*Massacand et al.*, 2001; *Martius et al.*, 2008). Elongated troughs are in fact precursors of heavy precipitation events in southern Switzerland(*Martius et al.*, 2006, 2008). The eastern flank of these, so called PV streamers, are regions for upper-level dynamical forcing for ascent (*Hoskins et al.*, 1985), favoring convective precipitation (*Massacand et al.*, 2001).

As an example, a case study by *Grams and Blumer* (2015) has established the role of TC Katia's interaction with the midlatitude waveguide in September 2011 and the subsequent downstream formation of a PV streamer. Warm and moist air was advected towards central Europe along the eastern flank of the PV streamer where high convective available potential energy (CAPE) was building up. Upper-level forcing for ascent ahead of the PV streamer led to deep convection and heavy precipitation over Germany. Simulations of the midlatitude flow evolution with a TC removal technique proved that no HIW event would have occurred without the interaction between the recurving tropical cyclone and the jet stream.

On the other hand, *Pantillon et al.* (2015) investigated the impact of 3 recurving North Atlantic tropical cyclones on downstream wave breaking during episodes of intense rainfall in the Mediterranean, in autumn 2012. This study states that the perturbation to a Rossby wave train over the North Atlantic by a recurving TC leads to a relatively weak remote impact compared to idealized simulations or North Pacific ET events (*Harr and Dea*, 2009; *Quinting and Jones*, 2016). Hence, the authors suggest that the chain of events leading to the observed downstream wave breaking would also happen without TC - jet interactions. They conclude that rather than a precursor of heavy rain events, interactions between recurving TCs and the jet act as a perturbation, relocating the precipitation events in space and time (*Pantillon et al.*, 2015).

Research on recurving tropical cyclones is highly motivated by these downstream high impact weather events. However, as mentioned, the attribution of remote extreme precipitation events to recurving tropical cyclones remains a debated question.

1.2.4 Reduced predictability after TC - jet interactions

The complexity of the interaction between a recurving tropical cyclone leads to increased forecast uncertainties for the downstream development of the midlatitude flow (*Anwender et al.*, 2008). Although Rossby wave packets have been associated with increased atmospheric predictability (*Grazzini and Vitart*, 2015; *Teubler and Riemer*, 2016), forecast errors have been linked to a misrepresentation of the effect of diabatic processes on the large-scale flow evolution in NWP models (*Grams et al.*, 2011). Therefore, large forecast errors in the current NWP models have been documented after ET events. Hence, the prediction of associated high impact weather events remains very uncertain.

1.3 Aims of the study and Research questions

In summary, previous studies have established the role of recurving tropical cyclones in the modification and downstream amplification of the midlatitude flow pattern. Current conclusions suggest that this amplification of the midlatitude flow can trigger high impact weather events downstream. However, HIW events have only been attributed to TC - jet interactions in individual case studies. There is currently no climatological evidence that recurving tropical cyclones interacting with the jet would lead to a systematic increase in downstream severe weather events. A climatological analysis of the downstream response to ET events in North Western Pacific has been conducted for the first time by *Archambault et al.* (2013) and confirmed statistical evidence of an increased waviness of the downstream midlatitude flow. However, this study did not involve high impact weather events.

Hence, given the current conclusions on the impact of recurving tropical cyclones, the aim of this study is to fill the gap of knowledge concerning a climatological relation between recurving North Atlantic tropical cyclones and downstream precipitation extremes. To this end, the following questions are addressed:

- Are recurving North Atlantic tropical cyclones conducive to a systematic increase in downstream precipitation extremes?

To address this question we set up several hypotheses:
First, if precipitation extremes occur after an interaction between a recurving TC and the jet due to the amplification of a Rossby wave packet, the distance between the point of maximum interaction (cf. section 2.2.1) and the extremes should be a function of the wavelength of the Rossby wave packet and should thus remain relatively constant between all cases. Therefore, we analyze precipitation extremes relative to the location of the point of maximum interaction between a recurving TC and the jet. In other words, the precipitation extremes will not be assessed over a defined location on Earth, but rather in a grid box located at a specific distance from the known maximum interaction point for each case. Hence, the following questions is addressed:

- Where do precipitation extremes occur after TC - jet interactions?
- What is a typical time lag between the interaction and the occurrence of precipitation extremes?

A second hypothesis is that the configuration of the jet at the moment of the interaction plays a crucial role in the development of the Rossby waves downstream of the interaction. Consequently the response in precipitation extremes may differ fo different configurations. To verify this second hypothesis, this last question is addressed:

- Do we see significant differences in the precipitation patterns for different flow types?

In the following section, the methods used to answer these questions are presented. A description of 3 study cases is then presented in chapter 3 to illustrate the chain of events following a TC - jet interactions. Finally, results of the study are presented and discussed in chapter 4.

Chapter 2

Data and Method

2.1 Data

This study is based on the European Center for Medium-Range Weather Forecasts (ECMWF) Reanalysis dataset ERA-Interim (*Dee et al.*, 2011). The original dataset, available at a T255L60 spectral resolution, is interpolated to a $1^\circ \times 1^\circ$ latitude-longitude and in the vertical to isentropes and pressure levels. Here we use the data from 1979 to 2013.

Furthermore, the IBTrACS (International Best Track Archive for Climate Stewardship) database (*Knapp et al.*, 2010) is used to retrieve 6-hourly TC positions and the onset timing of extratropical transitions. The IBTrACS database merges storm information from multiple meteorological centers to create a global best track dataset and is available to the public. The dataset has been retrieved from the National Oceanic and Atmospheric Administration (NOAA) Climate Data Record website (`https://www.ncdc.noaa.gov/ibtracs/`).

Finally, GridSat-B1 infrared data (*Knapp et al.*, 2011) from the NOAA Climate Data Record (`https://www.ncdc.noaa.gov/gridsat/`) is used for a visual analysis of the cloud top heights in case studies of different events. The GridSat-B1 data provides different infrared window channels. The 11 µm channel is used in this study.

2.2 Method

2.2.1 Identification of TC-jet interactions

One essential task in the assessment of precipitation extremes after the recurvature of tropical cyclones, is to define an objective metric for the interaction between the TC and the midlatitude waveguide. This metric will be then used to determine the interaction onset. Various definitions and methods have been used in previous studies, either based on the recurvature time or cyclone phase-space parameters (e.g. *Hanley et al.*, 2001; *Hart and Evans*, 2003; *Studholme et al.*, 2015). However, these methods focus mainly on structural changes of the transitioning storm. They do not take the interaction with the jet into account and are not automated (*Kofron et al.*, 2010). In this study, however, we are specifically interested in the interaction between a recurving tropical cyclone and the jet, regardless of the current state of the cyclone.

Archambault et al. (2013) used the negative PV advection by the irrotational (i.e., divergent) wind as a metric of the strength of the interaction between the TC and the jet stream; hereby assuming that the divergent part of the flow in the TC outflow region is mainly attributable to the TC itself. Here, the metric is therefore computed in a similar manner to *Archambault et al.* (2013) but on isentropic surfaces[1]. It is computed as follows:

$$PV_{adv} = -\vec{V}_{\chi} \bullet \nabla_{\theta}\ PV \tag{2.1}$$

$\vec{V}_{\chi}$ represents the irrotational part of the TC's wind field. $\nabla_{\theta}\ PV$ represents the potential vorticity gradient on an isentropic surface. The negative PV advection is the dot product of these two components (*Archambault et al.*, 2013). It is calculated on isentropic surfaces between 325 and 355K with a 5K increment and then vertically averaged.

The outflow of the TC, hereby, advects low PV air in the direction of the waveguide and leads therefore to large absolute values of negative PV advection. This metric is therefore used to objectively determine the onset of the interaction between a TC and the jet stream in this study. It has been shown that, although several mechanisms contribute

[1]This adapted metric has been developed and provided by Jacopo Riboldi, *Institute for Atmospheric and Climate Science, ETH Zürich*

to the interaction, the TC's outflow impinging on the midlatitude waveguide plays a determining role for the amplification of midlatitude Rossby waves (*Anwender et al.*, 2008; *Grams and Archambault*, 2016).

In order to identify the TC - jet interactions, TC positions are retrieved from the IBTrACS database. All TCs recurving under a latitude of 45°N are considered. Negative PV advection is computed in a 25° by 20° box (with a 1° x 1° resolution) around the TC from -48 hours until +144 hours relative to the recurvature time. At each time step, the minimum value inside this 25° by 20° field is retrieved. Finally, the minimum of these minimums represents the moment of the strongest interaction between the TC and the extratropical jet. It is, thus, defined as the interaction onset (t = 0). The coordinates of this minimum value represent the point of maximum interaction (see figure 2.1).

Between 1979 and 2013, 147 cases of tropical cyclones recurving below 45° have been identified in the North Atlantic.

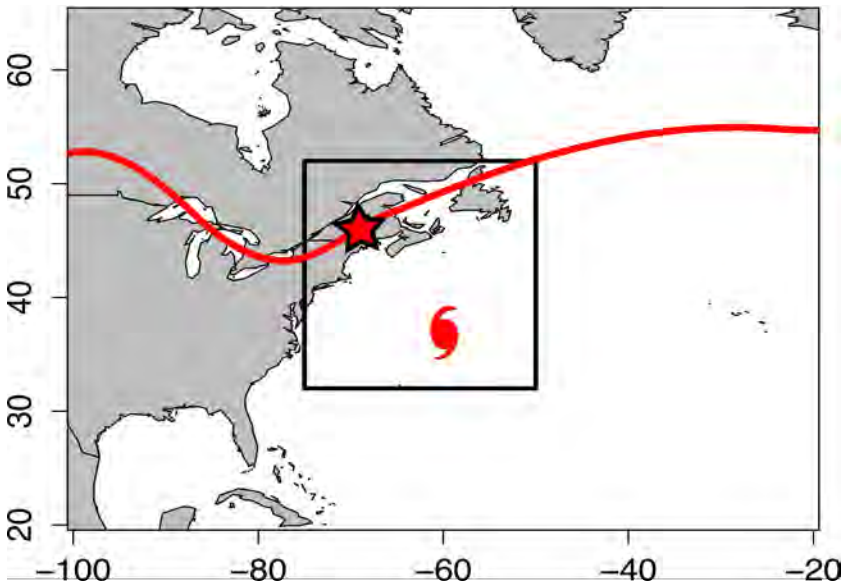

Figure 2.1: Schematic of an idealized TC - jet interaction. The red line represents the isentropic 2PVU contour colocated with the extratropical jet stream. The black box represents an area of 25° by 20° around the recurving TC, in which negative PV advection is calculated. The boundaries of the box are located 15° W, 10° E and 15° N, 5° S relatively to the storm. The star represents the minimum value of negative PV advection (= point of maximum interaction). (*Archambault et al.*, 2013).

Bare in mind that this study focuses on the timing of the strongest interaction between a recurving TC and the jet. The metric that is used has the advantage to be an objective definition to determine the interaction maximum. However, the interaction usually begins

before this peak in intensity and therefore, one can usually already see the effects of the approaching TC a few time steps earlier. Moreover, although this study does not focus on structural aspect of the cyclones (wether they are undergoing an extratropical transition or whether the transition has already been completed), the term "extratropical transition (ET)" may be used as a synonym of the interaction between a recurving TC and the jet in the following chapters.

2.2.2 Extreme precipitation analysis

This study considers daily precipitation accumulations. The value at a given time represents the accumulated precipitation in the preceding 24 hours. A precipitation extreme is considered as precipitation accumulation exceeding the climatological 99th percentile of the respective month's precipitation distribution (the 99th percentile is calculated from 6-hourly shifted daily precipitation values).

To study the effect of recurving TCs on precipitation extremes, binary fields with extreme events (benign values) denoted by 1 (0), are produced for every 6-hour time step. Composite maps of precipitation extremes of all study cases are compiled. The precipitation extremes are assessed with respect to the location of the points of maximum interaction between the TCs and the jet. Thus, maps of precipitation extremes are rotated around the pole, so that all points of maximum interaction are located on a same reference longitude (lon* 0°) before adding all the fields together. This operation is repeated for time lags 0 to 168h relative to t = 0 and in 6-hour time steps. Hence, time lagged precipitations extremes composites with respect to the points of maximum interaction are analyzed to identify the region with the highest development of precipitation extremes concentration (Section 4.1.1).

In a second step, one region of interest is retained for the study. The region of interest is a squared box with zonal boundaries located systematically 60 and 83° E from the points of maximum interaction and latitudinal boundaries at 35 and 52° N (see figure 4.2, section 4.1.1). Precipitation extremes in this box are assessed with two different metrics. First, the fraction of the area covered by extremes is calculated. All grid points with precipitation extremes within the box are first weighted with respect to their latitudinal

location and then summed up and divided by the total surface. This operation is repeated for each ET case for lags 0 to 168h relative to t = 0 and in 6-hourly time steps. Finally, a time series representing the average fraction of the box recording precipitation extremes is constructed (see section 4.1.

A second measure to assess the severity of precipitation extremes takes into account the volume of accumulated precipitation exceeding the threshold used to identify the extremes. Instead of binary fields, for this method, fields are produced with 0 for benign precipitation values and the exceedances of the 99th percentile (in mm) at grid points with extremes. Thereafter, the method is analogous to the first one. The final result is a time series of total accumulated water above the 99th percentile in a column with a 1° by 1° surface area (at the Equator). As for now, the first metric will be referred to as "precipitation extremes area" and the second metric: "precipitation extremes magnitude".

2.2.3 K-means clustering of PV fields

A visual analysis of 40 cases of recurving tropical cyclones interacting with the midlatitude waveguide put in evidence a large diversity in cyclones' locations and jet stream configurations (see section 3). Consequently, the response in terms of Rossby wave perturbation and precipitation extremes development is also highly diverse. One hypothesis in this study, is that the form of the jet stream upstream and downstream of the point of maximum interaction plays a role in the following events. Therefore, to verify this hypothesis and determine the importance of the midlatitude flow configuration, the studied cases have been first analyzed all together and then separated into 4 different clusters. Each cluster represents a different initial form of the jet stream at the moment of the interaction between the TC and the jet (see figure 4.8, section 4.2). To define the different clusters, a k-means clustering algorithm was applied to the PV fields around the points of maximum interaction.

For each case, a binary isentropic PV field around the point of maximum interaction was extracted. PV values smaller than 2 are reattributed a value of 0 and values greater or equal to 2, a value of 1. Thus, values of 0 represent tropospheric air on the corresponding isentrope and values of 1, represent stratospheric air. Only binary fields are considered

as we are only interested in the location and form of the troughs and ridges relatively to the point of maximum interaction.The cluster domain covers an area from -40° to +60° relative to the longitude of the maximum interaction point and -20° to +20° relative to its latitude. The isentropic level is selected depending on the month of the year as in *Röthlisberger et al.* (2016), so that the 2PVU line is colocated with the midlatitude jet.
The binary PV fields are used to perform the k-means clustering. Hereby, they are first converted into vectors and Euclidian distances are used to calculate distances between each case and the centroids. This operation is repeated a 1000 times. The most stable clusters are identified by selecting the clusters which are most similar across all 1000 repetitions.
The choice of the parameter k is based on the visual analysis and the total number of events. The analysis was also carried out with k = 3, but we lost one clearly distinct type of flow situation. Hence, k = 4 was a more relevant choice.
The analysis of precipitation is then conducted for each cluster in order to identify if one specific jet configuration is more conducive to the development of precipitation extremes. Potential vorticity composites for each cluster are presented in figure 4.8, section 4.2.
Note that hereby, the PV fields have been selected relative to the position of the respective point of maximum interaction.

2.2.4 Statistical testing: a bootstrapping method with analog flow situations

A bootstrapping method is applied to assess the statistical significance of the precipitation extreme response to the TC-jet interaction. However, a conventional bootstrapping method, would select purely random dates. This would not help to prove the role of the TC - jet interaction on the precipitation extremes, as TC - jet interactions often occur during an already amplified midlatitude flow. In fact, the increase in precipitation extremes could simply be caused by the natural evolution of the rather wavy midlatitude flow during TC - jet interactions. However, if by replacing the 147 cases of TC - jet interaction by other days with a similar flow situation, we find an increase of precipitation extremes, it would mean that the increase is caused by the flow situation itself and not

by the TC - jet interaction. On the other hand, if one does not observe any precipitation extremes increase with similar flow configurations, it would mean that an increase after tropical cyclones' recurvatures is indeed a result of the interaction with the jet and its subsequent flow amplification.

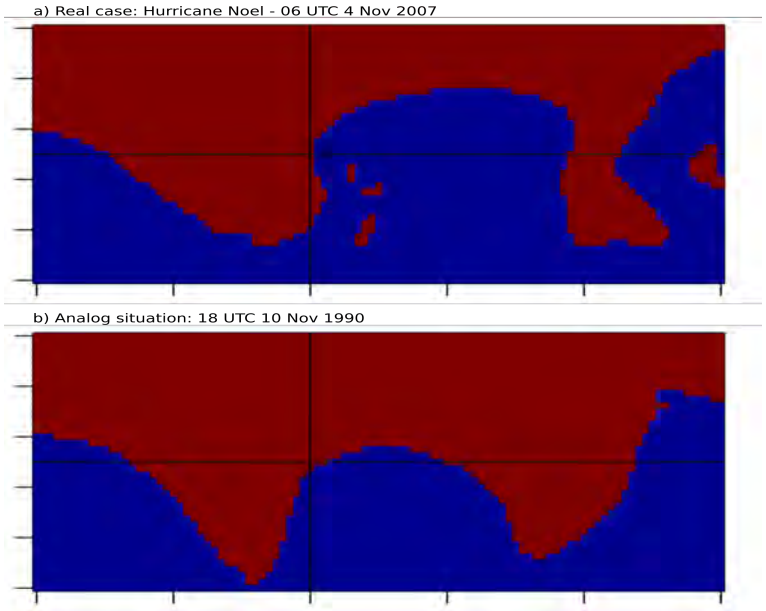

Figure 2.2: Illustration of a flow situation at the moment of strongest interaction between a recurving TC and the jet (panel a) and its analog (panel b) on the 325K isentrope. The red and blue colors represent respectively stratospheric (values above 2 PVU) and tropospheric (values below 2 PVU) air on this isentrope. The jet is located at the interface between the blue and the red. The point of maximum interaction is located (absolute maximum of negative PV advection) is located at the center of the cross on panel (a).

Selection of analog flow situations The similarity of flow situations is assessed by looking at the geometry of the isentropic 2PVU contour corresponding to the jet stream (see figure 2.2). For each recurving TC, the binary PV field around the point of maximum interaction is considered (as in the section 2.2.3). A grid placed on the same coordinates is considered at every 6-hourly time step for the period 1979-2013. Each flow situation (every 6-hours) is compared to the reference flow situation. As for the k-means clustering, the binary fields of potential vorticity are converted into vectors. Euclidian distances are computed to measure the distance between the reference PV field and every potential analog candidate. An analog flow situation has to occur during the same month as the real case in order to keep the same intra-annual distribution during the bootstrapping. The

two days preceding and the two days following any TC -jet interaction case are removed from the potential candidates. Finally, flow situations with the smallest distances (2^{nd} percentile) to the real case are retained (about 82 analogs per case).

Bootstrapping Each case has an attributed bin of analog flow situations with no approaching tropical cyclone. The bootstrapping consists in creating a sample by randomly selecting one analog in each bin. A time series of the average precipitation extremes in the sample is then computed as in section 2.2.2. This operation is repeated a 1000 times. We obtain a thousand time series of average precipitation extremes from random samples and compute the confidence intervals of these 1000 time series. Hence, we obtain the climatological precipitation response to a sample of midlatitude flow configurations similar to the TC - jet interactions' sample (see chapter 4).

2.2.5 Composite anomalies

In order to explain and support the results of downstream precipitation extremes, time lagged anomalies of condensational heating (CH), potential vorticity (PV) and integrated vapor transport (IVT) are used. Anomalies of each variable are computed by comparing time lagged composites from the 147 study cases to an average background field constituted of 1000 random composites from the bin of analog flow situations. For the composites, each map is rotated around the pole so that the respective points of maximum interaction are located along the same reference longitude (lon* 0). The latitudes remain constant to avoid distance biases due to Earth's curvature. Hence, the flow evolution is systematically analyzed downstream of the points of maximum interaction. Anomalies in the composites indicate the difference in the evolution of the midlatitude flow between cases with a recurving tropical cyclone and analog flow situations with no tropical cyclone interacting with the jet.

For potential vorticity, the isentropic level is selected separately for each case depending on the month of the year as in *Röthlisberger et al.* (2016), so that the 2PVU line is colocated with the midlatitude jet. Condensational heating is calculated on pressure levels and averaged between 1000 hPa and 300 hPa. It is expressed in [K/6h]. Integrated vapor transport is expressed in $[kg \cdot m^{-1} \cdot s^{-1}]$, calculated on pressure levels and inte-

grated between 1000 hPa and 300 hPa. These 3 combined variables represent the key ingredients for precipitation extremes development. Condensational heating, used as a surrogate for diabatic heating indicates processes leading to Rossby wave amplification, positive anomalies of potential vorticity indicate regions of stratospheric air intrusions and upper-level forcing for ascent (eastern flank of troughs) and IVT indicates availability of water for condensation and precipitation (cf. section 1.2).

Chapter 3

Case studies

A preliminary analysis of TC tracks and precipitation patterns following the recurvature of tropical cyclones showed that within all cases, the variability in the cyclones' locations and in the various meteorological fields were responsible for an important variation in the downstream development of the midlatitude flow and precipitation extremes. Hence, a visual analysis of over 40 cases helped to identify potentially important parameters for the development of precipitation extremes. The following section will illustrate some of these differences through a description of 3 example cases. These 3 cases present different initial set-ups and different precipitation patterns following the TC - jet interactions.
The extratropical transitions of Hurricanes Klaus (1984), Wilma (2005) and Leslie (2012) and the subsequent midlatitude flow evolutions are discussed with a 24-hourly sequence of the relevant variables (Figures 3.1, 3.2 and 3.3). Additionally, Figure 3.4 shows the track of each cyclone. The following life cycle overviews are based on the tropical cyclone reports provided by the National Hurricane Center (*Pasch et al.*, 2006; *Stewart*, 2013; *Lawrence and Clark*, 1985).

3.1 Hurricane Klaus - November 1984

Mid-West Atlantic interaction with an upstream trough and a long-wave downstream ridge

Tropical storm Klaus formed south of Puerto Rico from a low pressure system at 22 UTC, 6 November 1984 (not shown). It first kept a northeastward track into the Atlantic and strengthened along this track. At 00 UTC, 8 November 1984, it reached Hurricane strength (not shown). Two days later, at 00 UTC, 10 November 1984, Klaus was located at 23.8° N and 57.8° W and approached a baroclinic zone (*Knapp et al.*, 2010). An upper-level trough (T1) was located to the northwest of the cyclone, extending below the 30° N latitude and a ridge (R1) was located directly downstream of it. The ridge was covering most of the Atlantic and downstream a trough with a large meridional amplitude was located over Western Europe (not shown). 12 hours later (12 UTC, 10 November 1984), negative PV north of the cyclone indicates that its upper-level outflow was impinging on the extratropical jet.

At 00 UTC, 11 November 1984, maximum interaction occurred as Klaus was located at 29.5° N and 53° W with an SLP of 971 hPa (*Knapp et al.*, 2010). The point of maximum interaction was located at 41° N and 52° W with a value of -14.3 PVU/day[1](Figures 3.1a and 3.4) . From this moment, Klaus began its extratropical transition and weakened during the transforming stage (*Lawrence and Clark*, 1985). Grey shadings on Figure 3.1a indicate a developing jet streak right downstream of this point, which can be interpreted as a result of the increased PV gradient induced by the cyclone's upper-level outflow (*Archambault et al.*, 2013). The upstream trough began to wrap up anticyclonically around the transforming TC (Figure 3.1a), which is a favorable condition for cyclone re-intensification (*Ritchie and Elsberry*, 2007). A cirrus cloud shield expanding to the northeast along the jet is an indicator of Klaus' transforming stage (*Klein et al.*, 2000) (Figure 3.1c). This case has the particularity that it reached its maximum interaction intensity before the TC recurved.

At 00 UTC, 12 November 1984, a new ridge-trough couplet (R2-T2) had formed over

[1]PV advection is not plotted on Figures 3.1, 3.2 and 3.3

the Atlantic. The trough (T2) was located just downstream the cyclone (Figure 3.1d). Although, the meridional amplitude of this couplet was not yet very large, figure 3.1e exhibits a plume of large IVT (Integrated vapor transport) values from the Atlantic to the British Isles (up to 700 $kg \cdot m^{-1} \cdot s^{-1}$) and convection on the eastern flank of the trough (Figure 3.1d), which led to precipitation extremes over Ireland (Figure 3.1f). The preceding ridge-trough couplet (R1-T1) further amplified and the trough cut off over the western Mediterranean (Figures 3.1d,f), before being reattached to the main body of stratospheric air 12 hours later. This PV cutoff was associated with precipitation extremes over the Mediterranean region for 4 days. 12 hours later (12 UTC, 12 November 1984), Klaus reached its recurving point and began to track eastward with an increased translating speed (*Knapp et al.*, 2010). Klaus was located at 35° N and 55° W with an SLP of 984 hPa.

At 00 UTC, 13 November 1984, the new ridge (R2) had amplified and was covering most of the North Atlantic. The downstream trough (T2) had extended southward to 35° N with its eastern flank passing over Spain. Upper-level forcing for ascent on the eastern flank of the trough (T2) (Figure 3.1g) and moisture fluxes from the Atlantic (Figure 3.1h) led to precipitation extremes over Spain for 60 hours, while precipitation extremes kept occurring around the Adriatic sea, on the eastern flank of trough (T1) (Figure 3.1i).

Klaus eventually merged with another extratropical cyclone just above the North sea (*Lawrence and Clark*, 1985) and brought substantial amounts of precipitation to Portugal, Spain and France between 18 UTC, 14 November and 18 UTC, 16 November 1984 (Figure 14).

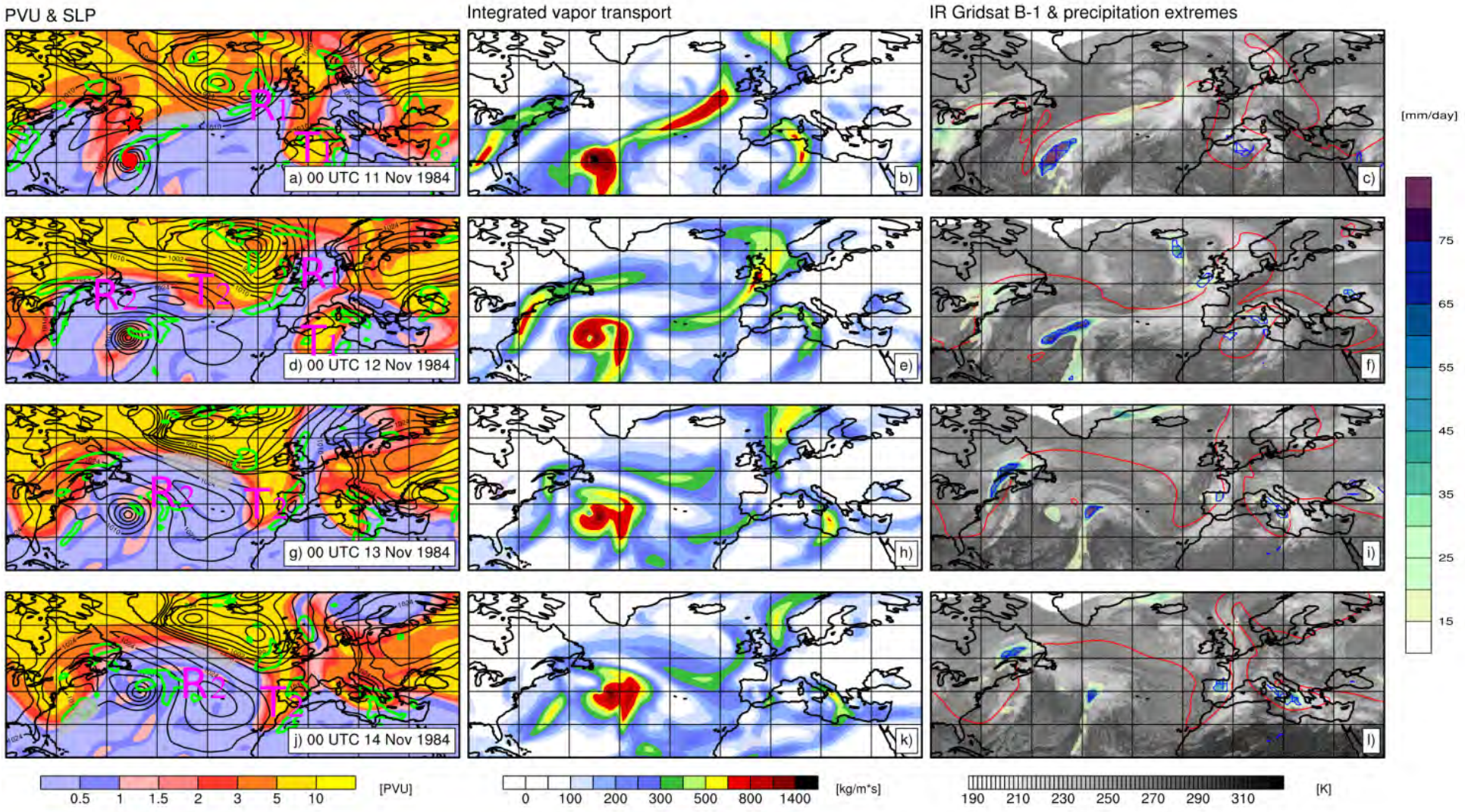

Figure 3.1: Hurricane Klaus' overview: Panels (a-d-g-j): potential vorticity at the 335 K isentropic surface in [PVU] (1 PVU = $10^{-6} \cdot K \cdot m^2 \cdot s^{-1} \cdot kg^{-1}$), horizontal wind at 335K above 55, 65 and 75 [m/s] (grey shadings) and ascending air at 500 [hPa] larger than -0.3 [hPa/s] (green contours). Panels (b-e-h-k): Integrated vapor transport in $[kg \cdot m^{-1} \cdot s^{-1}]$. Panels (c-f-i-l): IR satellite images of brightness temperature near 11 microns in [K], daily accumulated precipitation [mm/24h] and precipitation extremes (blue hatches). The red star on panel (a) represents the point of absolute maximum negative PV advection.

3.2 Hurricane Wilma - October 2005

Low-latitude west-Atlantic interaction with an upstream upper-level trough and a relatively zonal downstream flow

On 15 October 2005, Wilma's surface circulation and deep convection became well-enough defined to be classified as a tropical depression. After a short period of weak intensity and slow southward translation, Wilma turned northwestward on the 18th of October and started to intensify very rapidly until reaching category 5 only 24 hours later. It then continued on its track and made landfall over the Island of Cozumel, Mexico at 2145 UTC, 21 October 2005 and the Yucatan peninsula 6 hours later; causing severe damage and casualties. After emerging into the Gulf of Mexico, just north of the Yucatan peninsula, Hurricane Wilma recurved at 00 UTC, 23 October towards Florida and started to get closer to the extratropical jet (*Pasch et al.*, 2006). Between 00 UTC, 23 October and 00 UTC, 24 October 2005, a well amplified upper-level trough had formed over the United States and extended all the way to the Gulf of Mexico (Figure 3.2a). At 00 UTC, 24 October 2005, Wilma's upper-level outflow impinged on the midlatitude waveguide and led to a sudden increase of the absolute negative PV advection north of the cyclone. At this stage, Wilma was still considered a tropical cyclone with a central pressure of 958 hPa at sea level (*Knapp et al.*, 2010). A jet streak developed just to the north of the tropical cyclone and an extratropical cyclone was deepening at the same time at the left exit of this jet streak, just off the coast of Nova Scotia (see Figure 3.4 for the complete track).

At 18 UTC, 24 October 2005, the interaction between Wilma and the jet stream reached its maximum with a negative PV advection of -17.8 PVU/day. The point of maximum interaction was located at 39° N and 82° W and the cyclone at 28° N and 78.8° W (Figure 3.2a). At this time, the upper-level flow was characterized by a distinct upstream trough as mentioned above and a weakly amplified flow downstream. However, two low-amplitude ridge-trough couplets could be observed between 40 and 50° North over the Atlantic. Each trough was associated with an extratropical cyclone labeled T1 and T2 on Figure 3.2a. Figure 3.2b depicts a plume of strong moisture fluxes from the tropical

cyclone, all the way to northern Europe. At the same time, the jet streak over Wilma had strengthened as a result of increased horizontal PV gradient (Figure 3.2a).

One day later (00 UTC, 25 October 2005), Wilma was located at 40.5° N and 63.5° W with a central pressure of 976 hPa, just 370 km southeast of Nova Scotia (Figure 3.2, second row). The ridge located directly downstream of the cyclone had amplified and the associated trough (T1) had extended beyond the 40° N latitude. The extratropical cyclone co-located with the trough (T1) deepened explosively and the jet streak extended over the entire ridge from South Carolina, over the Island of Newfoundland to the mid-Atlantic (Figure 3.2d). The second extratropical cyclone moved over the coast of Norway. At 00 UTC, 26 October, Wilma was declared an extratropical cyclone (*Pasch et al.*, 2006). At 18 UTC, Wilma had moved to 45.5° N and 52° W. The T1 trough continued to extend southward with its eastern flank located along the 20° W longitude (Figure 3.2g). Two regions of convection can be observed on figure 3.2g on the eastern flank of the trough and large plumes of moisture are transported from the south (Figure 3.2h). Consequently two regions of extreme precipitation are colocated with the areas of convection (Figure 3.2i).

At 18 UTC, 27th of October, the trough (T1) had moved to the east (Figure 3.2j), bringing precipitation extremes to Portugal and western Spain for two days (Figure 3.2l). The northern patch of precipitation extremes passed right above the British Isles.

In conclusion, Wilma's extratropical transition triggered an amplification of the midlatitude flow and daily precipitation extremes over Portugal and Spain, between +48 and +96 hours after the moment of maximum interaction. However, most of the extreme precipitation occurred over the Atlantic ocean.

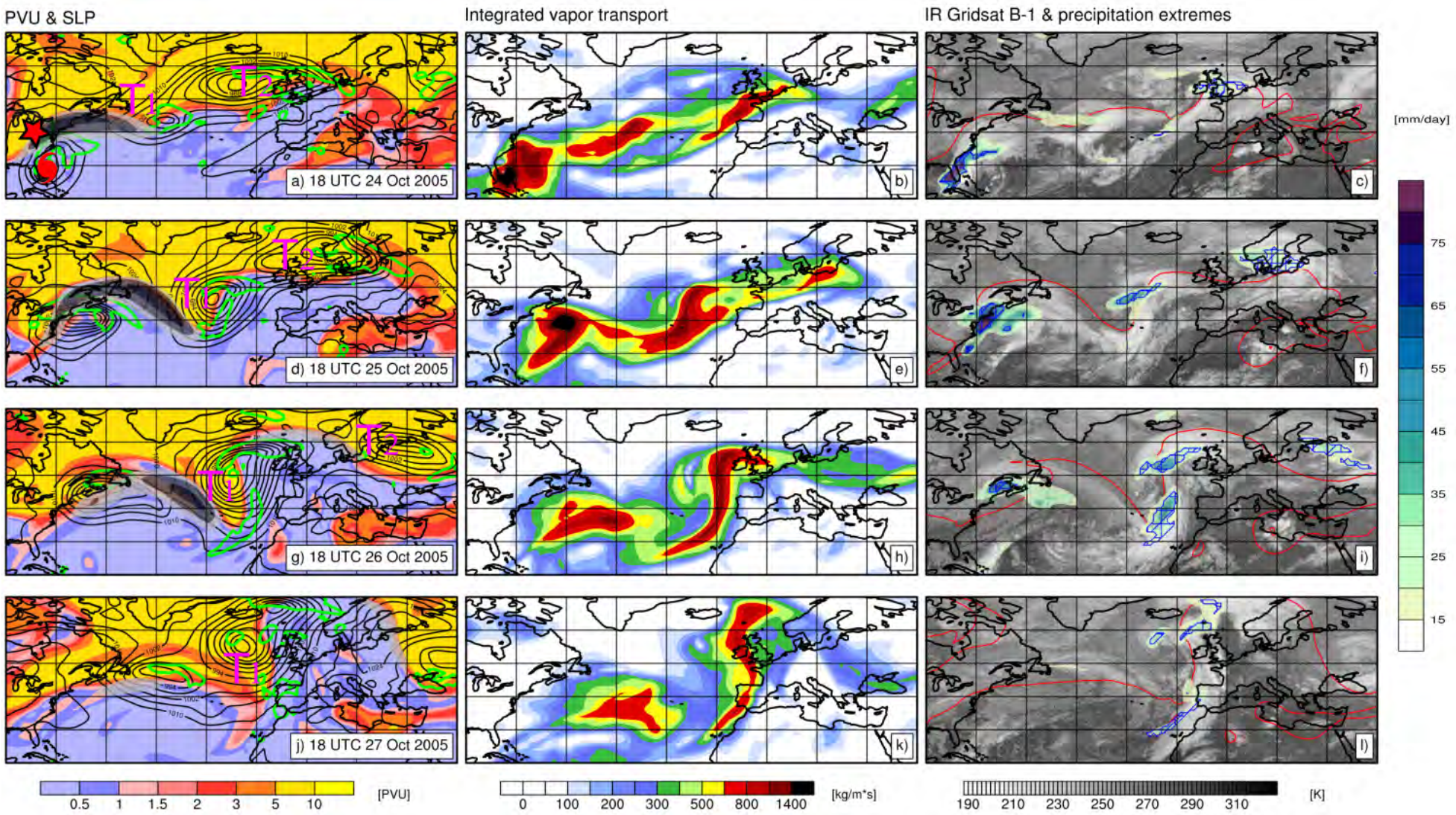

Figure 3.2: Hurricane Wilma's overview: Panels (a-d-g-j): potential vorticity at the 335 K isentropic surface in [PVU] (1 PVU = $10^{-6} \cdot K \cdot m^2 \cdot s^{-1} \cdot kg^{-1}$), horizontal wind at 335K above 55, 65 and 75 [m/s] (grey shadings) and ascending air at 500 [hPa] larger than -0.3 [hPa/s] (green contours). Panels (b-e-h-k): Integrated vapor transport in $[kg \cdot m^{-1} \cdot s^{-1}]$. Panels (c-f-i-l): IR satellite images of brightness temperature near 11 microns in [K], daily accumulated precipitation [mm/24h] and precipitation extremes (blue hatches). The red star on panel (a) represents the point of absolute maximum negative PV advection.

3.3 Hurricane Leslie - August/September 2012

West Atlantic interaction with amplified ridge-trough couplet downstream over the Atlantic

Leslie formed from a large easterly tropical wave that moved off the African west coast on 26 August 2012. It was classified as a tropical depression for the first time at 00 UTC 30 August 2012 as it was located at 13.5° N and 39.2° W, about 2400 km east-southeast of the northern Leeward Islands (*Knapp et al.*, 2010). Leslie maintained a west-northwestward track until early 3 September, while reinforcing and reaching tropical storm status. It then turned north-northwestward and slowed down. It maintained a slow motion for about 6 days (it briefly reached category 1 Hurricane) and began to accelerate again by early 9 September. It regained intensity and reached again category 1 Hurricane at 12 UTC 10 September at 36.4° N, 60.8° W. On 11 September, as it was approaching a baroclinic zone, Leslie encountered unfavorable environmental conditions for tropical cyclones. Thus, the hurricane began a transition into a strong extratropical cyclone (*Stewart*, 2013) (see figure 3.4 for complete track).

At 00 UTC, 11 September 2012 (Figure 3.3, first row), Leslie's interaction with the extratropical jet reached its peak. The cyclone and the point of maximum interaction were respectively located at 41.1° N, 58.6° W and 49° N, 66° W (Figure 3.3a). The midlatitude flow was characterized by an upstream trough over the East Coast of the United States and an amplified flow downstream of the cyclone. A downstream ridge (R1) associated with a surface anticyclone was covering almost the entire North Atlantic, extending beyond the 60° N latitude. It was followed by a thin and elongated trough (T1) with a North-East to South-West orientation and cut off 12 hours later over the Atlantic. On Figure 3.3a, a marked jet streak, with winds exceeding 65 m/s, can be observed just to the North of Leslie. Strong values of moisture fluxes occur on the southern flank of the jet streak (Figure 3.3b). During the following 24 hours, the upstream trough was wrapped up cyclonically around the cyclone and Leslie was officially classified an extratropical cyclone at 09 UTC 12 September 2012 (*Stewart*, 2013).

At 00 UTC, 12 September 2012, Leslie had moved over the Labrador sea, roughly 500

km south off Greenland (Figure3.3d). The downstream ridge (R1) was then extending north of the 65° N latitude and the jet streak had moved to the eastern flank of the ridge. The PV cutoff from the trough remained over the Atlantic but no precipitation extremes were associated with it (Figure3.3f). 6 hours later (06 UTC, 12 September 2012), Leslie officially merged with another extratropical cyclone (*Stewart*, 2013).

At 00 UTC, 13 September 2012, the ridge (R1) had moved east, over the British Isles (Figure3.3g). The remnant of trough T1 began to re-elongate and formed a new trough (T2) over central Europe, reaching the northern Mediterranean. An area of active convection formed over northern Italy and eastern Europe and precipitation extremes occurred over Slovenia, Austria, Czech Republic and Poland (Figure 3.3i). IVT values of up to 600 $kg \cdot m^{-1} \cdot s^{-1}$ appear along the southern and eastern edge of the forming trough, located over the Mediterranean (Figure 3.3h).

During the following 24 hours, this trough continued to elongate and a low pressure system formed over Italy, which eventually transitioned into a cyclonic cut off at 18 UTC, 14 September 2012. At 00 UTC, 14 September 2012, ridge R1 was subject to strong shear between two air masses of high PV air and oriented southwest-northeastward over Europe (Figure 3.3j). A cyclone had formed just off the Italian west coast. Strong moisture fluxes over the Ionian and Adriatic seas associated with convection on the right hand side of the cyclone led to precipitation extremes over the Balkans (Figures 3.3k,l). These precipitation patterns remained over the region for 60 hours.

This scenario is similar to Hurricane Helene in 2006 (described by *Pantillon et al.* (2013)), a recurving cyclone in the North Atlantic, which triggered a Medicane over Italy several days later, even though no Medicane formed in this particular case.

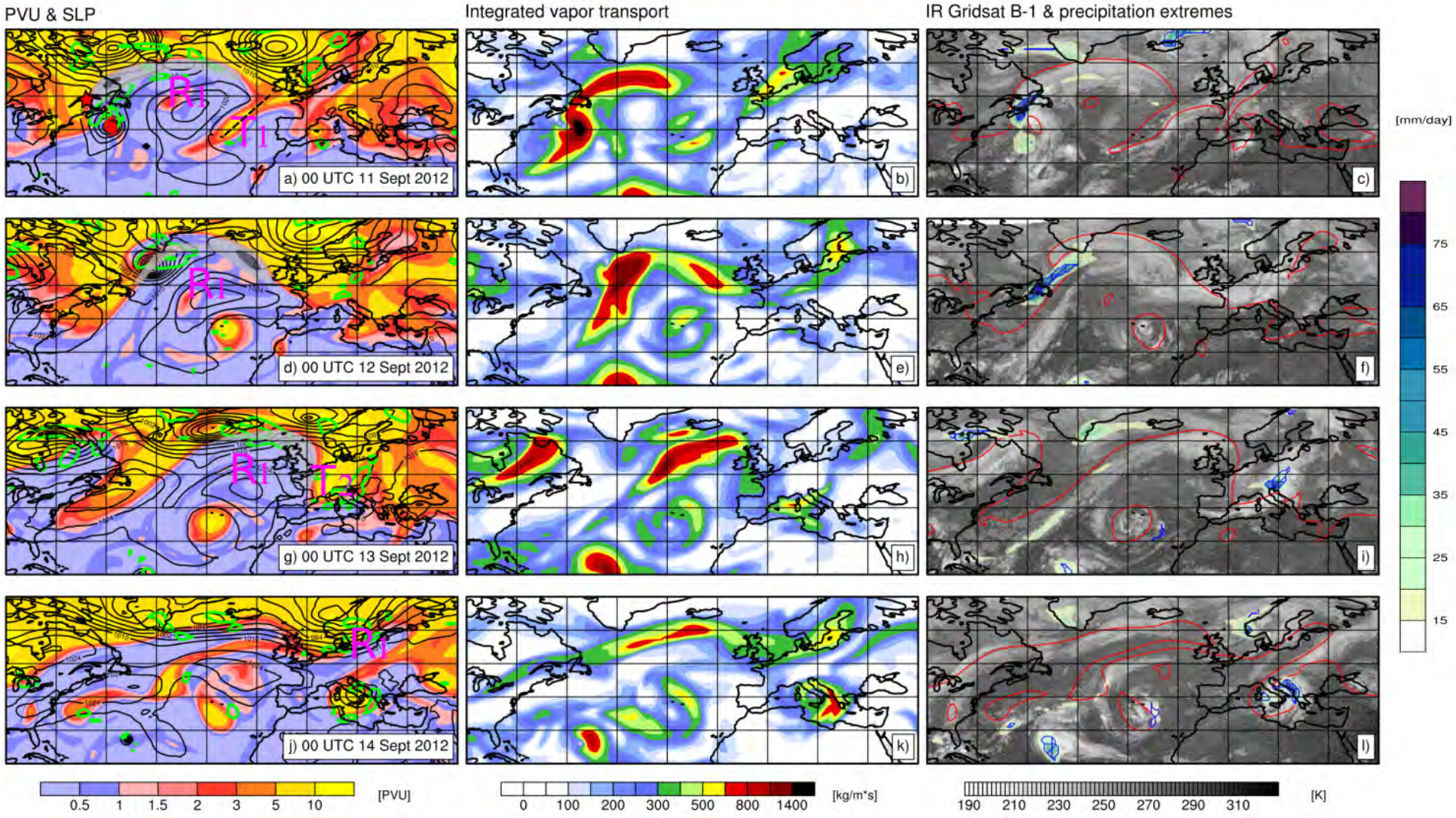

Figure 3.3: Hurricane Leslie's overview: Panels (a-d-g-j): potential vorticity at the 335 K isentropic surface in [PVU] (1 PVU = $10^{-6} \cdot K \cdot m^2 \cdot s^{-1} \cdot kg^{-1}$), horizontal wind at 335K above 55, 65 and 75 [m/s] (grey shadings) and ascending air at 500 [hPa] larger than -0.3 [hPa/s] (green contours). Panels (b-e-h-k): Integrated vapor transport in $[kg \cdot m^{-1} \cdot s^{-1}]$. Panels (c-f-i-l): IR satellite images of brightness temperature near 11 microns in [K], daily accumulated precipitation [mm/24h] and precipitation extremes (blue hatches). The red star on panel (a) represents the point of absolute maximum negative PV advection.

3.4 Synthesis

The 3 cases presented in this chapter have been selected out of 40 cases, which have been thoroughly inspected. The idea behind this analysis was to describe different ways how recurving TCs could lead to precipitation extremes further downstream and also to illustrate the considerable variability and complexity of the the midlatitude flow during and after TC-jet interactions. This analysis revealed indeed how diverse the response could be. The evolution of the midlatitude flow depends on many factors, including the initial shape of the jet stream meanders but also the location of the TC, the presence of already existing extratropical cyclones and moisture fluxes.

In the 3 cases presented, one can clearly observe that each cyclone had a different track and thus, interacted with the jet stream at a different location in the Atlantic. Secondly, the configuration of the jet stream was also different but yet highly relevant for the subsequent precipitation extremes in each case. Therefore, these two elements will be taken into account for the analysis of precipitation extremes.

The next chapter will present the evolution of the precipitation extremes after TC - jet interactions. In a first step, precipitation extremes will be analyzed regardless of the flow situation during the interaction (precipitation extremes after all recurving TCs). After this initial analysis, a k-means clustering algorithm will be applied to PV fields (Section 2.2.3) in order to determine main flow types during TC - jet interactions. The influence of the flow type will then be assessed in order to determine which configuration is more conducive to precipitation extremes.

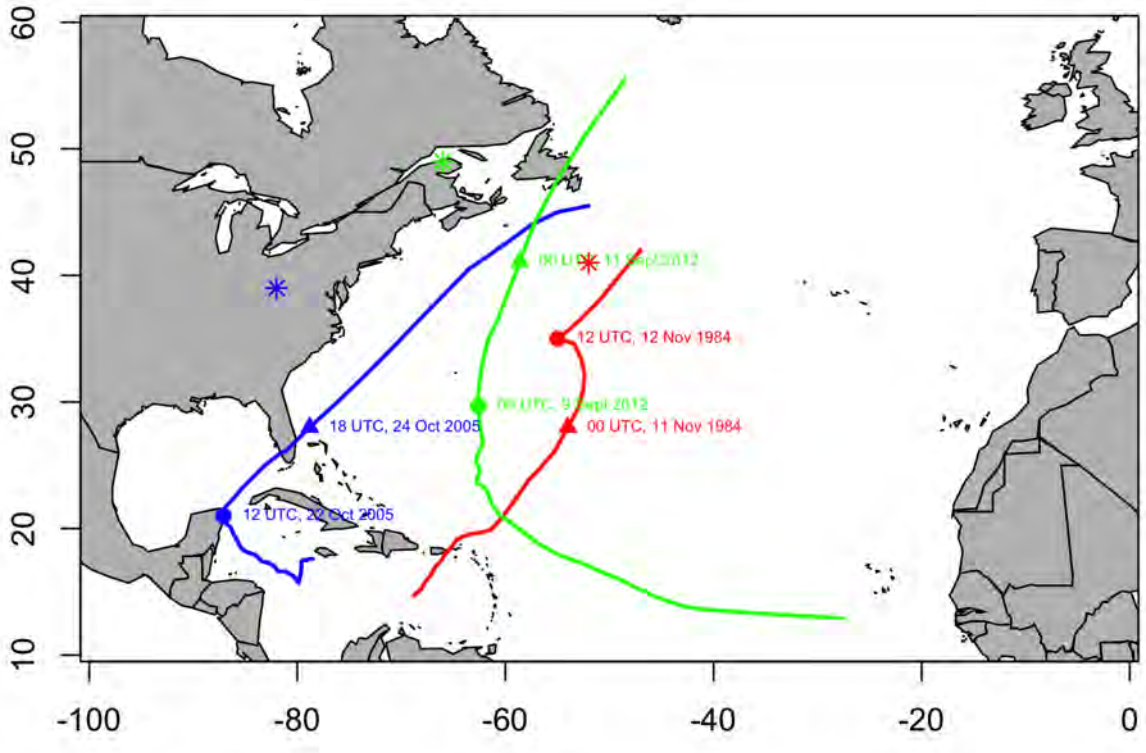

Figure 3.4: Tracks of tropical cyclones Klaus (red), Wilma (blue) and Leslie (green) retrieved from the IBTrACS dataset (*Knapp et al.*, 2010). The dots, triangles and stars respectively represent the recurvature points, locations of the cyclones at the moment of the strongest interaction with the jet and maximum interaction points.

Chapter 4

Precipitation extremes following TC - jet interactions

In this chapter, time lagged precipitation extremes following TC - jet interactions are analyzed and discussed. In addition, PV, IVT and CH anomaly maps are used to support the results and interpret the time and spatial scales of precipitation extremes. In a second part, the different initial flow types resulting from the clustering algorithm are presented and their different impacts on downstream precipitation extremes discussed.

4.1 Part I: Analysis for all recurving tropical cyclones

4.1.1 Time lagged precipitation extremes composites

On Figure 4.1, composites of precipitation extremes binary fields from the time of interaction onset until +72 hours, with 24-hourly increments show the general evolution of precipitation extremes after TC - jet interactions. The value at each grid point represents the number of times a precipitation extreme was recorded in 147 cases of TC - jet interactions. As a reminder, a precipitation extreme is a precipitation value exceeding the 99th percentile of its month precipitation distribution (cf. Section 2.2.2). Hence, for a purely random date, the probability of getting an extreme at a grid point is 0.01. If we select 147 random binary fields of precipitation extremes, the expected value at each grid point is therefore 1.47. An example of a purely random draw of 147 days is shown on Figure 1,

in the Appendices.

On Figure 4.1a, a concentrated plume of precipitation extremes, oriented south-north is located to the east of the reference longitude lon* 0. These precipitation extremes represent precipitation associated with the transition of TCs. Further downstream, precipitation extremes are relatively homogeneously distributed, with no apparent specific organization. 24 hours later (Fig. 4.1b), the precipitation extremes from the tropical cyclones are still visible, however shifted to the north-east. Between roughly 40 and 65° E, a southwest-northeast oriented patch of higher values of precipitation extremes can be observed. 48 hours after interaction (Fig. 4.1c), the remnants of the tropical cyclones appear as a southwest-northeast oriented band between 0 and 40° E. East of the 60° longitude, the previously observed patch of precipitation extremes seems to be more organized and concentrated. 24 hours later (Figure 4.1d), this plume of precipitation extremes remains visible. It has slightly moved to the east and is more scattered but clearly contrasts with the surroundings.

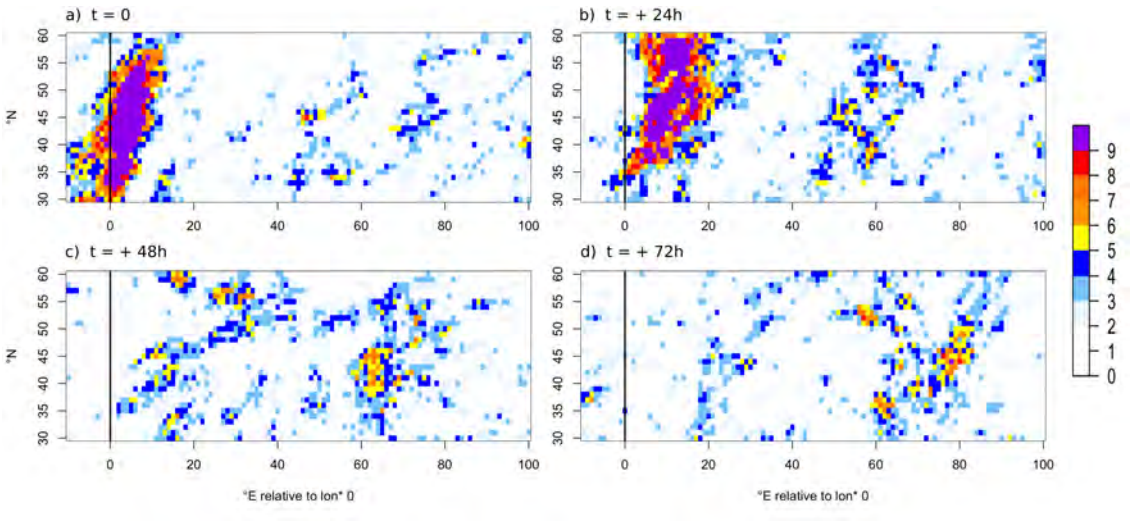

Figure 4.1: Time lagged precipitation extremes composites. The value in each grid point represents the cumulated number of extremes recorded within the 147 studied cases. All maps were priory rotated around the pole so that the points of maximum interaction are located along a same reference longitude. The vertical black line represents the reference longitude. Panel (a): t = 0 Panel (b): t = + 24h Panel (c): t = + 48h Panel (d): t = + 72h.

This observed plume of precipitation extremes can potentially be a response to the TC - jet interactions and the subsequent wave amplification. To analyze the precipitation extremes response to TC - jet interactions, a box has been assigned to the area where this plume appears. An illustration of this box is shown on Figure 4.2. Based on the average

location of all the points of maximum interaction, if this box was projected on a map, it would cover a region between 3° W and 20° E and 35° N and 52° N (i.e. Central Europe and the Mediterranean) (Figure 2, Appendices).

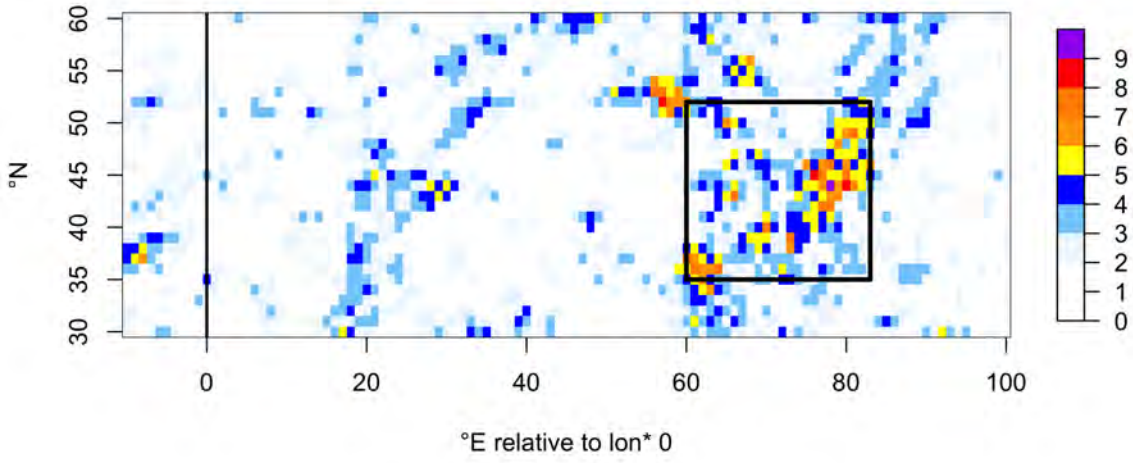

Figure 4.2: Precipitation extremes composites after 72 hours. Same as Figure 4.1d. The black box indicates the area investigated for precipitation extremes. The western and easter boundaries are respectively located 60° and 83° to the east of the maximum interaction point (black line), and hence move according to the location of the latter. The southern and northern boundaries are respectively located at 35° and 52° N. These latitudes remain constant in order to avoid a distance bias between the point of maximum interaction and the box due to earth's curvature.

Precipitation extremes are thus assessed within this delimited area as detailed in section 2.2.2. Results are presented in the following section.

4.1.2 Precipitation extremes time series

Figure 4.3 shows the evolution of precipitation extremes in the box defined above. Figure 4.3a depicts an increase in the area covered by precipitation extremes between +18 hours and +54 hours. It first peaks at +54 hours with 1.84% of the box covered by precipitation extremes and then, a second peak of 1.9% at +72 hours can be observed. It then slowly decreases and reaches values closer to the median of the bootstrapping distribution. Between +42 and +96 hours, the red line exceeds the 99^{th} percentile of the empirical precipitation extremes' distribution.

Note further that the bootstrapping distribution for the precipitation extremes' area re-

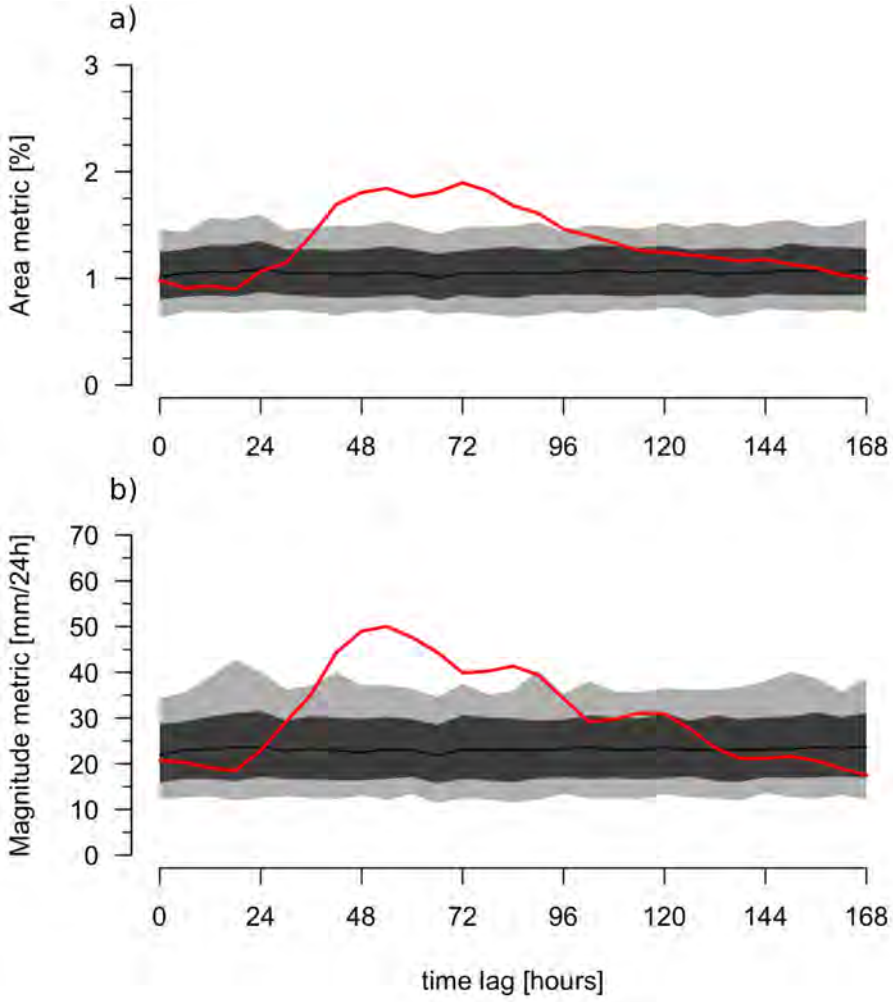

Figure 4.3: Time series of precipitation extremes after TC - jet interactions in the investigated box. Panel (a): The horizontal axis represents the time lag after TC - jet interaction onsets. The vertical axis represents "Area metric" (= fraction in [%] of the box covered by precipitation extremes at a given time after the interaction). Panel (b): The vertical axis represents the "precipitation extremes magnitude metric" in the box (= summed exceedances of climatological 99^{th} at each grid point in the box). The red line represents the average of 147 recurving TC events. The light and dark gray shadings respectively represent the empirical 1^{st}-99^{th} and the 10^{th}-90^{th} intervals of precipitation extremes obtained from the bootstrapping test. The black line represents the mean of the bootstrapping distribution. The bootstrapping distribution is composed of 1000 means. Each mean is composed of 147 analog situation (cf. Section 2.2.4).

mains relatively constant throughout the time series. As that the bootstrapping is based on cases exhibiting analog flow situations, this indicates that the observed increase is an effect of the recurving cyclones interacting with the jet rather than the pre-amplified flow at t = 0.

The precipitation extremes magnitude in the box exhibits a similar increase as the area covered with precipitation extremes (cf. Figure 4.3a,b). As a reminder, the magnitude metric represents the sum of precipitation accumulations at each grid point exceeding

their respective climatological 99th percentile. All exceedances in the investigated box are summed up in one water column with a 1° by 1° base (at the equator) and the magnitude metric represents the height of this water column (cf. Section 2.2.2). Events covering the same area can therefore be compared. A more intense event will consequently exhibit a greater value in the magnitude metric for a similar surface coverage.

The +54-hour peak (Fig. 4.3b) exhibits a value of 50 mm/24h while the bootstrapping mean displays a value of 23.2 mm/24h. The red line decreases then gradually until reaching same values as the bootstrapping mean at +132 hours. Based on this metric, we conclude that the precipitation extremes are more intense during the 24 hours preceding the 54-hour peak than during the 24 hours preceding the 72-hour peak (Figure 4.3a). Nevertheless, the accumulated water by precipitation extremes also remains above the empirical 99th percentile between +36 and +90 hours.

Hence, Figure 4.3 indicates that on average, the surface covered by precipitation extremes in the box almost doubles 30 to 72 hours after a TC - jet interaction and the magnitude metric is multiplied by 2.5.

An indication of the variability in precipitation extremes within the 147 recurving TCs is given in Figure 4.4 in the next section.

4.1.3 Variability of the precipitation extremes response to TC - jet interactions

Results of Figure 4.3 represent the average of precipitation extremes after 147 cases of TC - jet interactions. A first interpretation of these results, is to say that when the red line exceeds the empirical 99th percentile of the bootstrapping distribution, the average precipitation extremes following 147 TC - jet interactions is significantly different from the average precipitation extremes for any composite of 147 other days (with no preceding TC - jet interaction), at the confidence level alpha = 2%. However, despite this promising signal, this result doesn't tell if TC - jet interactions are systematically followed by such an increase in precipitation extremes. Therefore, Figure 4.4 provides an indication of the variability within the 147 analyzed cases by displaying a confidence interval of the precipitation extremes time series. The confidence interval for all analogs considered for

the bootstrapping test is also displayed.

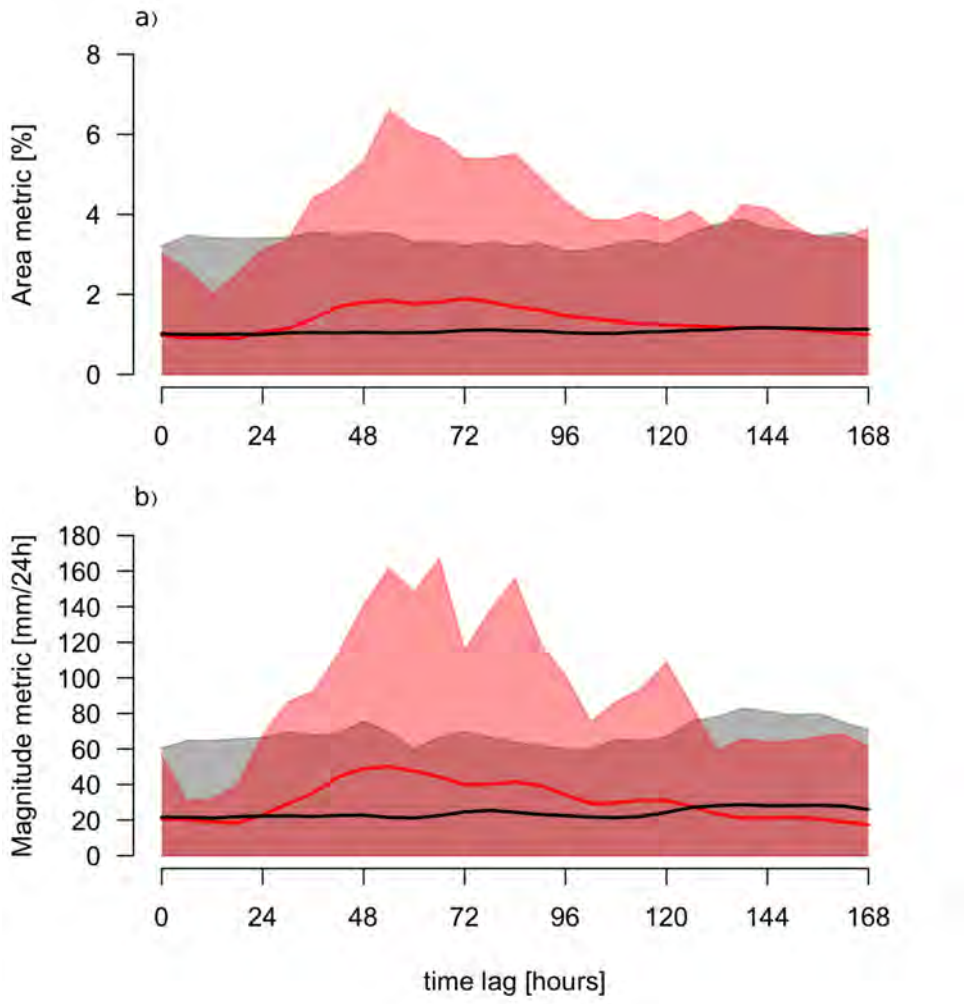

Figure 4.4: Time series of precipitation extremes after TC - jet interactions with 10-90th percentile confidence intervals. Panel (a) displays the average precipitation coverage (= Area metric) as in Fig. 4.3 (red line). The red shading represents the 10-90th percentile confidence interval of the 147 recurving TCs' sample. The black line represents the the average precipitation extremes coverage of the analog flow situation population. The grey shading represents the 10-90th percentile confidence interval of the entire analog flow situation population (12'054 cases). Panel (b) is the same but for the "magnitude metric" [mm/24 hours], representing the column height of summed exceedances of precipitation extremes thresholds in the investigated box (cf. Section 2.2.2).

A large variance is observed for both samples on each panel of Figure 4.4. The 90th percentile of the recurving TCs' sample (red shading, Fig. 4.4a) reaches a value of 6.6% (166 mm/24h, Fig. 4.4b) after 54 hours, but the lowest 10% of the sample indicate a value of 0% of the box covered by precipitation extremes (0 mm/24h for the magnitude metric). The variance is the largest during this peak. The confidence interval of the analog situations remains relatively stable in time with respective values for the 10th and

90^{th} percentiles of 0% (0 mm/24h) and $\sim$ 3.5% (60-80 mm/24h).

Bare in mind that the confidence intervals of analog situations samples (grey shadings) in Figures 4.3 and 4.4 do not represent the same thing. On Figure 4.3, the confidence interval represents the distribution of 1000 random sample means, with each sample being constituted of 147 analog situations from the entire population of analog flow situations (cf. Section 2.2.4). Figure 4.4 considers the distribution of all individual cases from entire population of analog flow situations. Therefore, the 10^{th} percentile of the bootstrapping distribution on Figure 4.3 remains above 0 because the cases with the lowest precipitation extremes values are compensated by cases with higher values, as we consider means. It is not the case on Figure 4.4, where the distribution clearly displays the cases with less precipitation extremes (or even no precipitation extremes at all).

The large variability in precipitation extremes of the TC - jet interaction sample observed on Figure 4.4a,b is however not a surprise. Based on the differences in initial flow conditions and key parameters for wave amplification within all recurving TC events, it is expected that a precipitation extremes increase would not necessarily happen in every case and would exhibit spatial and time variability.

As mentioned in Section 1.3, this study aims to find how often TC - jet interactions are followed by a precipitation extremes increase. To get a better estimate of which fraction of recurving TCs is followed by a precipitation extremes' increase similar to figure 4.3, a simple test has been conducted.

On Figure 4.3a, we can observe that the red line exceeds the 99^{th} percentile threshold of the bootstrapping distribution (grey shading) between +36 and +96 hours. During this period, the average precipitation extremes following the TC - jet interactions is significantly different from the average precipitation extremes for any composite of 147 other days (with no preceding TC - jet interaction). We subjectively define this period as a time window of interest. Hence, we seek cases that exhibit a significant increase in precipitation extremes during this time window. We define the 90^{th} percentile of the entire analog population's distribution as a threshold (grey shading on Fig. 4.4). Cases exceeding this threshold anytime during the time window are considered as cases that follow the same precipitation extremes pattern as the average observed on Figure 4.3. From now, these

cases are considered as "good" cases for the sake of comprehension. To be considered as "good", a case must meet the following criteria:

- The precipitation extremes metric must exceed the 90th percentile threshold of the entire analogs population's distribution at least once during the given time window.
- The precipitation extremes metric must be below this 90th percentile threshold at time 0 (interaction onset). This assures to select cases exhibiting an increase from an initially normal to a high amount of precipitation extremes.

The selection method is illustrated on Figure 4.5.

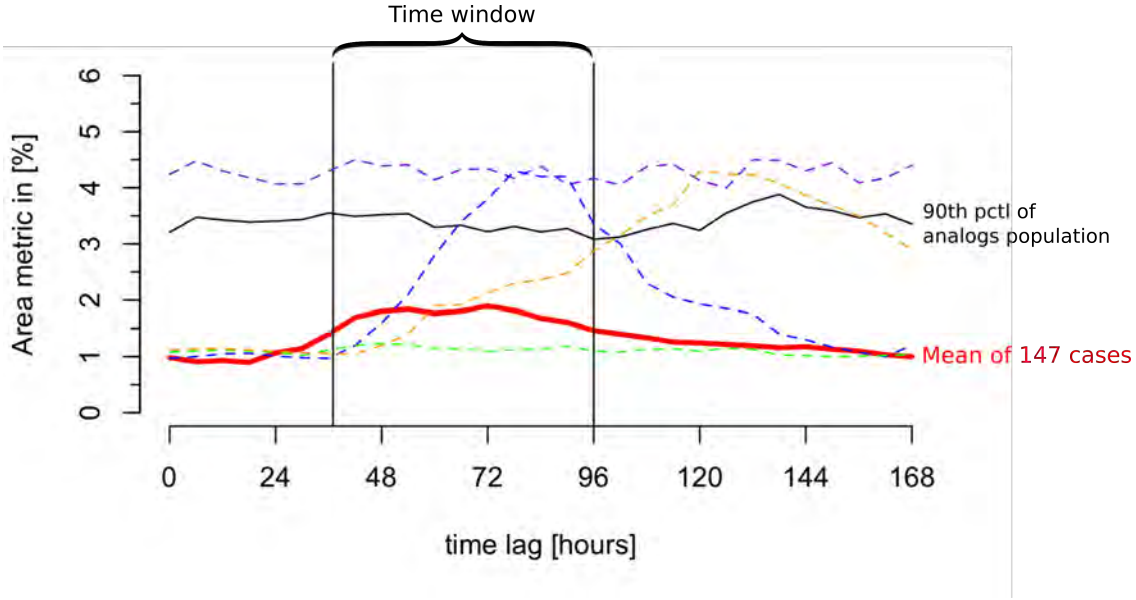

Figure 4.5: Illustration of identification method for "good" cases.

Although the purple dashed line (Fig. 4.5) exhibits precipitation extremes values above the 90th percentile threshold during the time window, it is not considered as a "good" case because the initial value (at t = 0) is also exceeding the threshold. Hence, these high values are not necessarily due to the TC - jet interaction. The green dashed line does not show any increase in precipitation extremes. The orange dashed line exhibits a significant increase in precipitation extremes. However, it exceeds the 90th threshold after the time window. The blue dashed line is a "good" case. Its initial value is below the threshold and it exceeds the threshold at least once during the time window. This method is used for both metrics with their respective thresholds to compute the proportions

of "good" cases within our sample of precipitation extremes time series following TC - jet interactions. For the area metric, 41.5% of recurving TCs are followed by such a precipitation increase pattern and for the magnitude metric, 41%.

To gain insight on the dynamical mechanisms leading to the spatial distribution and time scale of these precipitation extremes, time lagged anomalies of potential vorticity, integrated vapor transport and condensational heating are presented in sections 4.1.4 and 4.1.5.

4.1.4 Condensational heating composite anomalies

Here, global fields of vertically averaged condensational heating (from 1000 hPa to 300 hPa, in [K/6h]) are used as a surrogate for the full diabatic heating. Figure 4.6 presents condensational heating anomalies for a 5-day period in 24-hourly increments starting from the time of interaction onset. Anomalies are computed by comparing a composite of the 147 cases of recurving TCs sample to the average of 1000 composites of randomly selected samples (each sample has 147 elements) from the analogs population (cf. Section 2.2.5). In addition to the anomalies, the average location of the 2PVU contour (co-located with the extratropical jet) is indicated by a red line. The blue contour represents the location of the 2PVU line for the analog flow situations. Here again, the average of 1000 potential vorticity composites of randomly selected analogs is used to determine the propagation of Rossby waves with no TC - jet interaction (= background state).

On Figure 4.6a, the red contour exhibits an upstream trough and a downstream ridge, roughly 40° wide. The blue contour exhibits similar features, however, less amplified. This point will be discussed in Section 4.3.2. A 10°-wide band of positive CH anomaly oriented south-north can be seen just to the east of the upstream trough with maximum values exceeding 2.1 K/6h near 44° N and 5° E (Figure 4.6a). This south-north elongation is however mainly due to the latitudinal displacement of the maximum interaction points along the reference longitude (cf. vertical black line at 0°). In the next section, Figure 4.7a shows important positive anomalies of vapor transport collocated with these condensational heating anomalies. The warm and moist air is a major source for the diabatic processes along the baroclinic zone. The positive CH anomalies observed in Figure

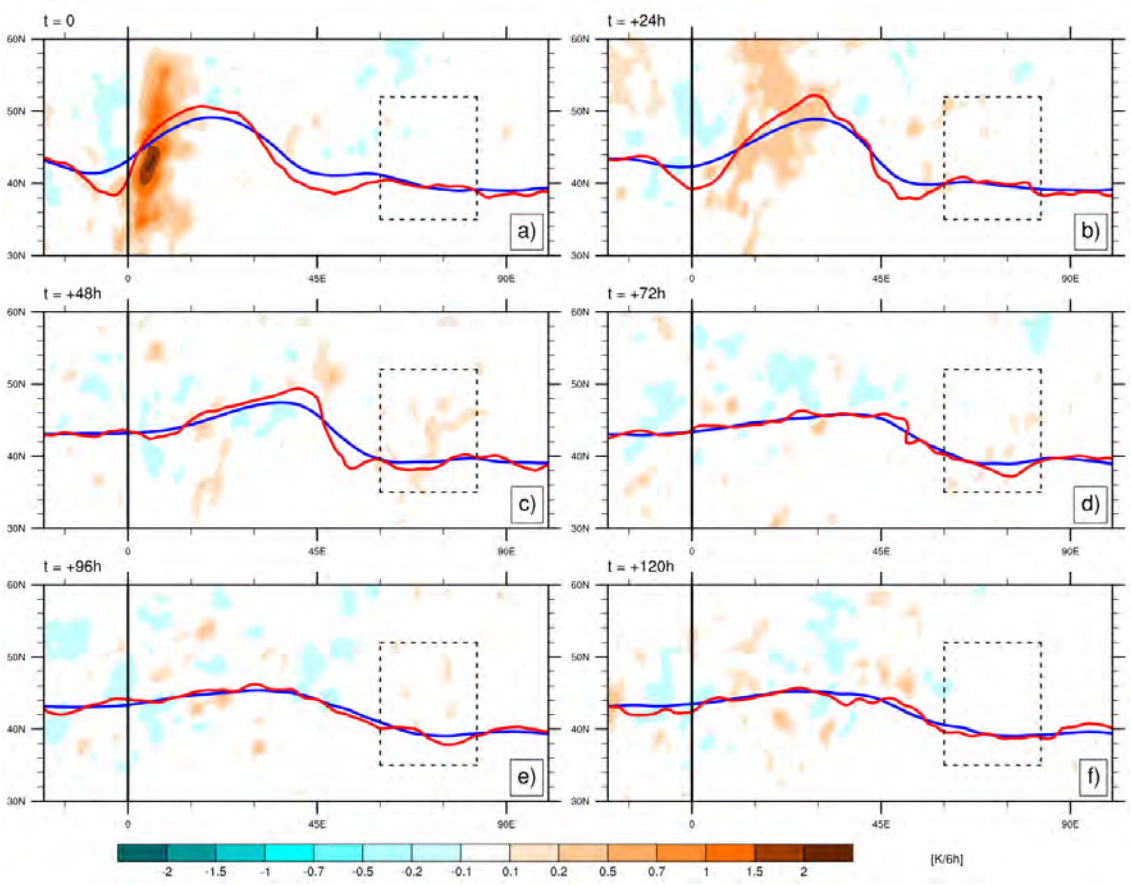

Figure 4.6: Condensational heating anomaly evolution after TC - jet interactions in [K/6h] (cyan-brown shadings). The red line represents the average isentropic 2PVU contour of the study cases. The blue line represents the average location of the 2PVU contour of the analog flow situations. Longitude 0 represents the location of the points of maximum interaction. The black square represents the area where precipitation extremes are investigated. Panel (a): composites at time 0. Panel (b): composites after 24 hours. Panel (c): composites after 48 hours. Panel (d) composites after 72 hours. Panel (e) composites after 96 hours. Panel (f) composites after 120 hours.

4.6 contribute to the downstream amplification of the flow (cf. Figure 4.7). 24 hours later (Fig. 4.6b), a large patch of positive CH anomalies can still be observed east of the upstream trough. However, the absolute values of the anomaly have decreased, probably because of the different evolutions of each recurving TC. We can see that the ridge-trough couplet has shifted to the east, both in the real (red line) and the analog situations (blue line) and the red line remains more amplified than the blue line. 48 hours later (Figure 4.6c), positive anomalies up to 0.2 K/6h can be observed downstream in the box. These anomalies are the signature of the condensation leading to precipitation extremes after TC - jet interactions. In the following 48 hours (Figure 4.6d,e), the positive anomalies in the box decrease and after 120 hours (Figure 4.6f), no more anomaly is observed.

This decrease corroborates the decrease in precipitation extremes after the 72-hour peak observed on Figure 4.3.

In summary, important condensational heating, near the midlatitude waveguide, occurs during the first 24 hours. This positive anomaly is explained by the presence of recurving tropical cyclones interacting with the jet. Diabatic processes described in section 1.2.2 occur during the interaction between a cyclone and the midlatitude waveguide. Between 48 and 72 hours later, positive anomalies of condensational heating are observed in the downstream box, indicating condensation processes leading to the recorded precipitation extremes.
Section 4.1.5 will present the evolution of the PV and IVT anomalies after the TC - jet interactions; two key variables for the development of precipitation extremes.

4.1.5 Potential Vorticity composite anomalies

In this next step, we discuss the evolution of potential vorticity and integrated vapor transport anomalies. Figure 4.7, displays the evolution of PV and IVT anomalies between the moment of interaction onset and 5 days later in a 24-hour sequence.
A large positive IVT anomaly is located just to the east of the upstream trough at t = 0 (Figure 4.7a). These strong moisture fluxes conceivably result from the proximity of approaching tropical cyclones. Moist air is transported towards the baroclinic zone and forced to ascend in this zone (cf. section 1.2.2). This results in positive anomalies of condensational heating as seen on Figure 4.6a. The upstream trough is followed by a ridge about 40° long (red contour). 24 hours later (Figure 4.6b), strong moisture fluxes are seen along the eastern flank of the trough, up to the crest of the downstream ridge. Indeed, a negative PV anomaly centered in 30° E is reinforcing towards the north of the map, just at the crest of the ridge. Further downstream, a new trough starts to form between 45 and 60° E. This trough is colocated with a positive PV anomaly and a positive IVT anomaly above 30 $kg \cdot m^{-1} \cdot s^{-1}$. In section 4.1.2, precipitation extremes were found to peak between 48 and 72 hours after interaction onsets. Since the daily precipitation values represent the preceding 24-hour accumulation, these high precipitations begin after 24 hours, which can be explained by the positive PV anomaly located just to the west

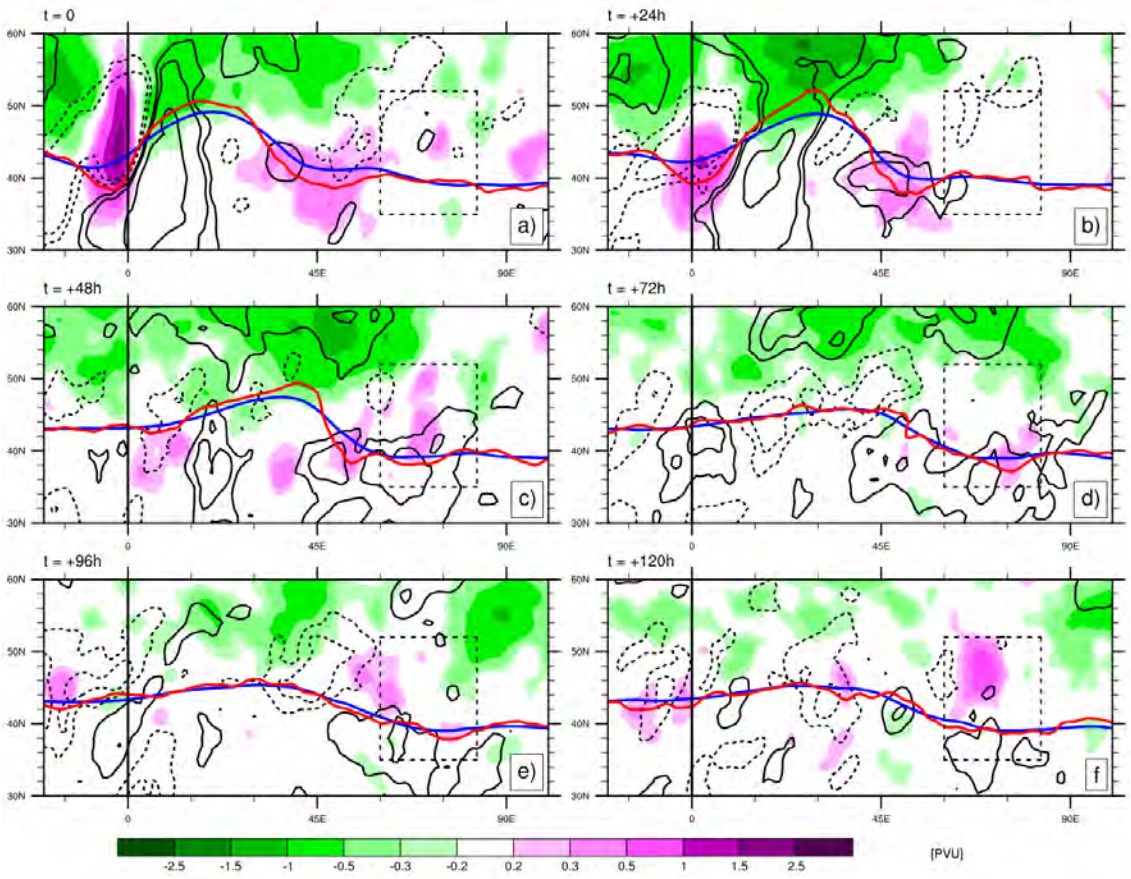

Figure 4.7: Potential vorticity and integrated vapor transport anomaly evolution after TC - jet interactions. Purple (green) shadings indicated positive (negative) potential vorticity anomalies in [PVU]. Full (dotted) black contours represent positive (negative) IVT anomalies of -90, -30, -15, 15, 30 and 90 $[kg \cdot m^{-1} \cdot s^{-1}]$. The red line represents the average isentropic 2PVU contour of the study cases. The blue line represents the average location of the 2PVU contour of the analog flow situations. Longitude 0 represents the location of the points of maximum interaction. The black square represents the area where precipitation extremes are investigated. Panel (a): composites at time 0. Panel (b): composites after 24 hours. Panel (c): composites after 48 hours. Panel (d) composites after 72 hours. Panel (e) composites after 96 hours. Panel (f) composites after 120 hours.

of the grid box and this positive IVT anomaly after 24 hours. On Figure 4.7c, positive PV anomalies patches can still be observed in the grid box and to its left, along with positive IVT anomalies. However, no clear trough appears in the composite 2PVU line. On panels (d),(e) and (f), the meridional amplitude of the 2PVU line gets reduced. The magnitude of the IVT and PV anomalies also decreases. This corroborates the decrease in precipitation extremes after the 72-hour peak (cf. section 4.1.2). This decrease of waviness of the 2PVU line can be explained by the large variety of initial flow situations amongst all recurving TC - jet interaction cases. The different initial flow situations have different responses after the interactions, and therefore, the waves do not follow the same

evolution. Hence, when computing composites, the different PV fields cancel each other out and the result is a flat 2 PVU contour. The same anomaly analysis has been made after a clustering of the initial flow situations and the evolution of more similar initial conditions is presented in section 4.2.4.

4.2 Part II: Influence of different flow types

Despite a large variability amongst the studied cases, the analysis of the surface and magnitude of precipitation extremes presented in section 4.1.2 shows promising results. Nevertheless, as mentioned in section 1.3, the initial flow situation is certainly an important feature for the amplification and dispersion of Rossby waves and the occurrence of precipitation extremes further downstream. To elaborate on the role of the extratropical flow configuration during the TC-jet interaction, a k-means clustering algorithm has been applied to the PV fields at the time of interaction onsets (cf. section 2.2.3 for the method) in order to cluster these flow configurations in distinct groups. Based on visual inspection of the identified clusters as well as based on the synoptic analysis of the 40 cases, we subjectively chose to separate the full set of TC-jet interaction cases into 4 clusters. The analysis of precipitation extremes has then been carried out for each of these flow types.

4.2.1 Identification of different flow types

Figure 4.8 displays the PV composites and size of each cluster. The point of maximum interaction is indicated by a cross. The first flow situation (Figure 4.8a) is composed of 21 members. It is characterized by a relatively narrow trough almost centered on the point of maximum interaction. This latter is located on the eastern flank of the trough, near the peak. A long wave ridge extends downstream over almost 60° of longitude and a meridional extent of about 15-20° to the north of the interaction point. An upstream ridge with a little less meridional amplitude is also visible. The second flow situation (Figure 4.8b) is composed of 54 members. It represents the most "zonal " jet configuration. It does however exhibit quite substantial variability on both sides (east and west) of the map. The jet forms a low-amplitude ridge-trough-ridge succession similarly to Figure 4.8a but with very low. Flow situation number 3 (Figure 4.8c) is marked by a strongly

amplified wave pattern. The point of interaction is located on the eastern flank of an upstream trough, which is broader than the trough in cluster 1 (Figure 4.8a). A large-amplitude ridge with a strong horizontal PV gradient is located to the east and followed by a trough with a southwest-northeast orientation. 32 members form this cluster. The forth flow situation represented on Figure 4.8d is characterized by a zonal jet to the west of the interaction point and a ridge downstream. The jet (to the west of the interaction point) is located at lower latitudes in comparison to the other flow types. This last cluster is constituted of 40 members.

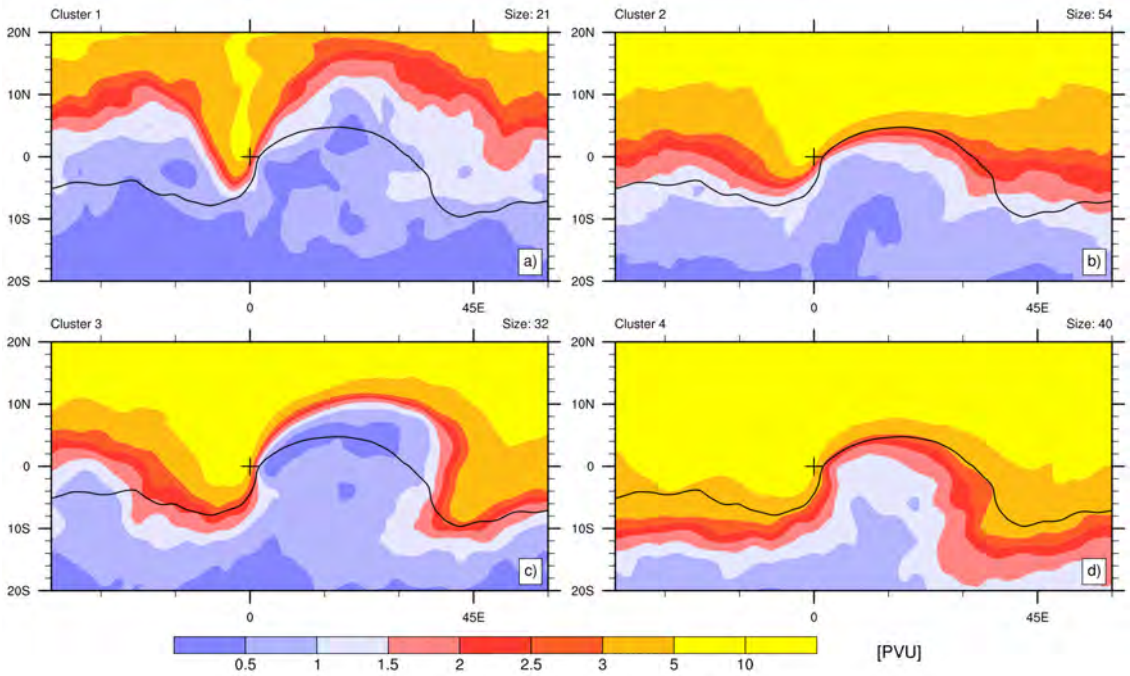

Figure 4.8: PV composites of each cluster in [PVU]. The black cross represents the location of points of maximum interaction between the TC and the jet. The black line represents the average location of the 2PVU contour for a composite of all cases for comparison. Panels (a): Cluster 1 - 21 members. Panels (b): Cluster 2 - 54 members. Panels (c): Cluster 3 - 32 members. Panels (d): Cluster 4 - 40 members.

Section 4.2.2 provides an analysis of the precipitation extremes evolutions after TC - jet interactions from each cluster.

4.2.2 Precipitation extremes after TC interactions with different initial jet configurations

In this section, we will apply the same method as in Section 4.1 (Part I) for each cluster separately. In Section 4.1.1, we used precipitation extremes composites to define an area

of interest that has been investigated. Here, composites are used to re-define a specific area of interest for each cluster (which differs from the initial box), as the initial flow situation also impacts on the location of the downstream precipitation extremes. (Results of precipitation extremes for each cluster in the initial box are presented in the Appendices for direct comparison.)

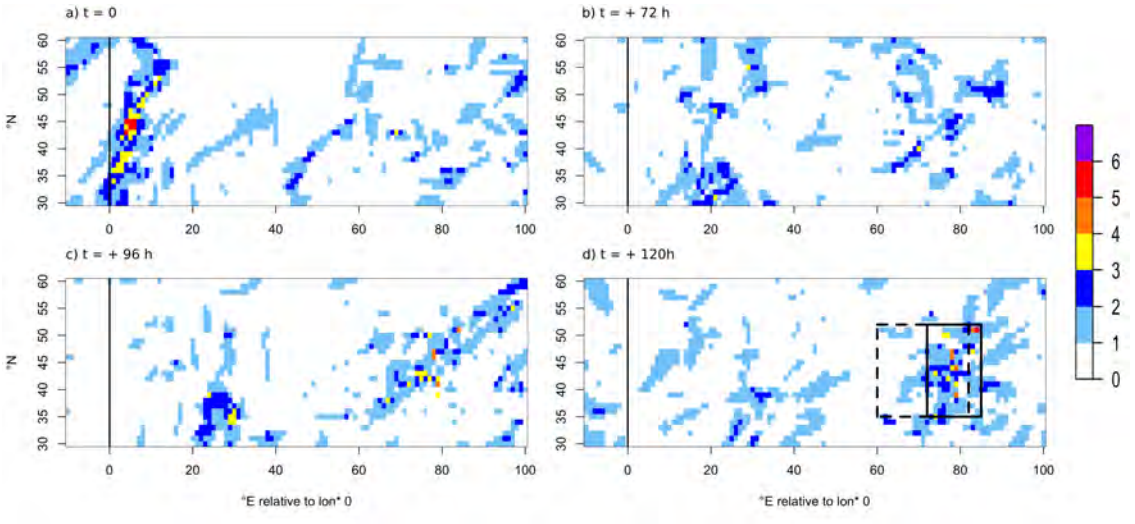

Figure 4.9: Time lagged precipitation extremes composites after TC - jet interactions from cluster 1. The value in each grid point represents the cumulated number of extremes recorded within the 21-case sample. All maps were priory rotated around the pole so that the points of maximum interaction are located along a same reference longitude. The vertical black line represents the reference longitude. The dashed black box on panel (d) indicates the area investigated in the previous section. The full line box indicates the new area of interest for cases from cluster 1. Panel (a): t = 0 Panel (b): t = + 72h Panel (c): t = + 96h Panel (d): t = + 120h.

Figure 4.9 shows precipitation extremes composites for cases from cluster 1. Figure 4.9a exhibits similar features to Figure 4.1. High values of precipitation extremes just to the east of the reference longitude and relatively low and homogeneous values downstream. On Figure 4.9c,d, (+96 and +120 hours) higher values of precipitation extremes are observed between roughly 70 and 85° E. Therefore, a new area of interest is defined between 72 and 85° E of the reference longitude and 35 to 52° N. This new box represents the eastern half of the initial box. For each cluster, the same operation is repeated (not shown here) and the area of interest selected for each cluster in presented on Figure 4.10. The evolution of precipitation extremes has then been analyzed for each cluster in its respective box. Results are presented in section 4.2.3.

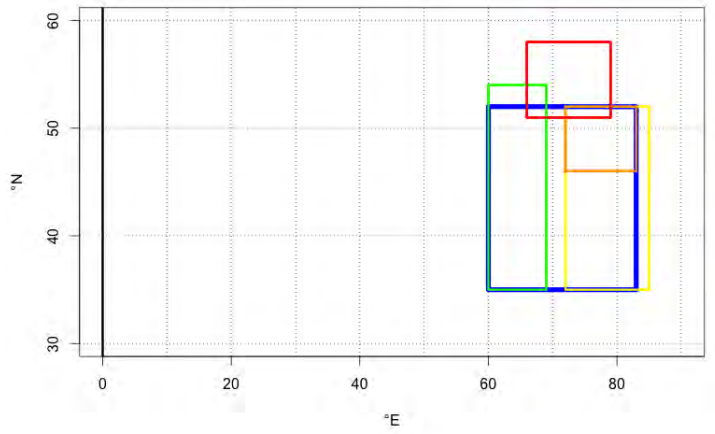

Figure 4.10: Sketch of box selection for precipitation extremes analysis. The spatial distribution of precipitation extremes differ for each cluster. Therefore, the precipitation extreme analysis is tested in different boxes for each cluster. The size of each box and its location is defined based on composites of precipitation extremes (cf. Appendices). The areas showing the largest values of extreme events serve to define the boxes. Blue box: 60° - 83° E and 35° - 52° N (all TCs), Yellow box: 72° - 85° E and 35° - 52° N (Cluster 1), Green box: 60° - 69° E and 35° - 54° N (Cluster 2), Orange box: 72° - 83° E and 46° - 52° N (Cluster 3), Red box: 66° - 79° E and 51° - 58° N (Cluster 4).

4.2.3 Precipitation extremes time series for different clusters

Figure 4.11 displays a time series of precipitation extremes after TC - jet interactions from cluster 1, in an adjusted box (cf. Figure 4.9d). Time series for clusters 2, 3 and 4 are displayed in the Appendices.

At first sight, Figure 4.11 exhibits a larger variance of the bootstrapping distribution (grey shadings). This could partly be explained by the effect of the jet stream's evolution for such initial configurations. However, since cluster 1 has only 21 members, it is most likely due to the smaller sample. Compared to Figure 4.3, precipitation extremes for cluster 1 exhibits a much later peak in both metrics. The maximum values are obtained at +120 hours with respective values of 4.19% and 85 mm/24h for each metric. Part of this increase in precipitation extremes can be explained by the normal evolution of the midlatitude flow, however, the recorded extremes greatly exceed the bootstrapping 99^{th} percentile during the peak. Hence, between 96 and 120 hours after TC - jet interactions from cluster 1, a 2.7 times larger area is covered by precipitation extremes and the magnitude metric is multiplied by 3.7 (compared to the mean of the bootstrapping distribution). Figures 12a and 13a (Appendices), show time series of precipitation extremes for cluster

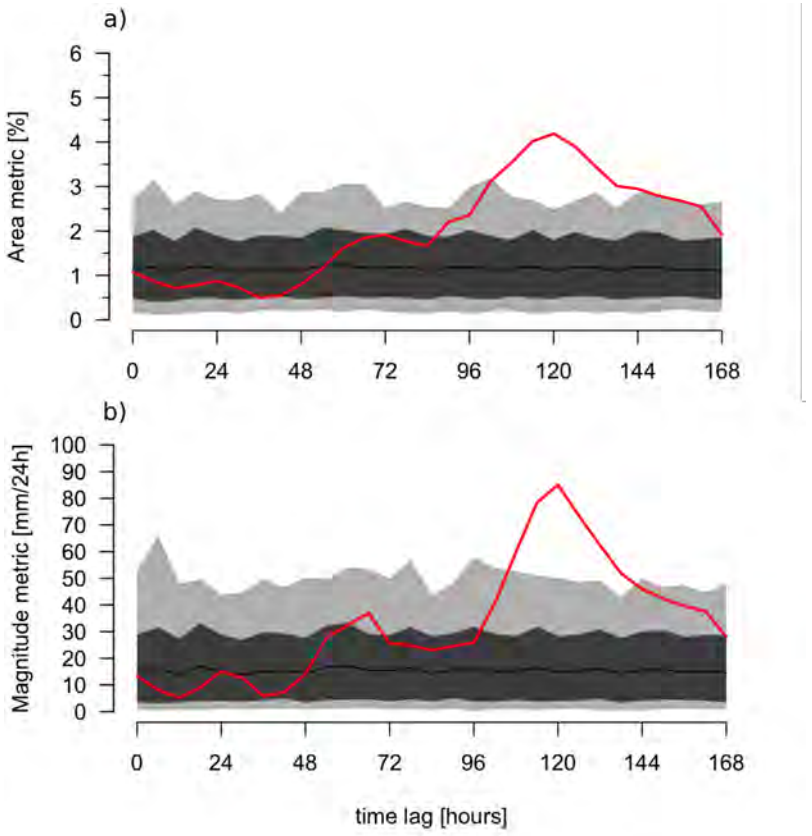

Figure 4.11: Time series of precipitation extremes after interactions from cluster 1 in a redefined grid box. Panel (a): The vertical axis represents the fraction in [%] of the new grid box recording precipitation extremes at a given time after the interaction. Panel (b): The vertical axis represents the magnitude metric in [mm/24h] in the new grid box. The red line represents the average of 21 recurving TC events. The light and dark gray shadings respectively represent the empirical 1^{st}-99^{th} and the 10^{th}-90^{th} intervals of precipitation extremes obtained from the bootstrapping test. The black line represents the mean of the bootstrapping distribution.

1 in the initial box (cf. Fig. 4.10), which covers roughly twice the same surface. For comparison, the 120-hour peak indicates values of 2.73% and 89.2 mm/24h for each respective metric. We notice that the magnitude metric is very close in both cases. Hence, the new box provides a more accurate indication of the location of the downstream precipitation extremes after TC - jet interactions from cluster 1. Based on the average location of TC - jet interaction points from cluster 1, the projection of this area on a map would on average be located between 9 and 23° E and 35 to 52° N, which would mainly cover Italy, the Balkans and most east European countries. Since the precipitation extremes after interactions from cluster 1 occur further downstream from the interaction point, it partly explains the longer time lag before the peak in precipitation extremes.

Although, part of the precipitation extremes in cluster 1 can be explained by the flow

situation itself (as seen from the bootstrapping distribution), the interaction with a recurving TC, significantly increases precipitation extremes in the respective box. Cases from cluster 1 lead to the heaviest precipitation events. These results corroborate the hypothesis that the response of the midlatitude flow after TC - jet interactions depends on the initial shape of the jet stream.
To determine what proportion of cases in cluster 1 are followed by the pattern observed on Figure 4.11, the same test as in Section 4.1.3 has been applied. Here, the time window during which, precipitation extremes must exceed a threshold, is between 102 and 144 hours after TC - jet interaction. 62% of cases from cluster 1 follow a similar pattern for both metrics of precipitation extremes (Fig. 4.11a,b).

Along with cluster 1, cluster 2 is followed by a significant precipitation extremes increase after TC - jet interactions. The area of interest for cluster 2 indicates that precipitation extremes are, in these cases, concentrated on the western portion of the original area (cf. Fig 4.10). The precipitation extremes peak between 48 and 54 hours after the interaction onset (cf. Figure 3). The surface fraction covered by precipitation extremes reaches 3.1% during the peak and the column height of the "magnitude metric" reaches 38 mm/24h. Hence, the surface coverage is tripled compared to the bootstrapping's distribution mean and the "magnitude metric" is almost quadrupled. This cluster is the largest, with 54 cases. Within these 54 cases, 41% follow a similar evolution for the first metric (cf. Fig. 3a) and 39%, for the second metric (cf. Fig. 3b).

Cluster 3 exhibits a very intense peak in precipitation extremes at 48 hours (cf. Fig. 6). However, the bootstrapping distribution exhibits more variance for this cluster. Since, this cluster represents the more pre-amplified flow situations, it could explain higher downstream precipitation values, even without a recurving TC. The precipitation extremes are concentrated to the northeast of the initial area, in a box about the forth of the size of the initial box. The peak at 48 hours indicates a surface coverage of 5.5% and a accumulation for the precipitation extremes magnitude of 24 mm/24h. However, the box for cluster 3 is smaller than boxes for cluster 1 and 2. 34% of cases from cluster 3 follow this pattern for the "area metric" and 46.8%, for the "magnitude metric".

Cluster 4 does not exhibit any particularly strong increase, even after several attempts of box redefinition. Figure 4.10 indicates one possible area of interest for precipitation extremes, but the increase remains relatively weak. Results for precipitation extremes in the initial area of interest (Fig. 12 and precmmgroups) are more interesting, as they contribute more to the general tendency observed in Section 4.1.2.

We recall that in Section 4.1.3, we found that 40.8% of all cases were following a similar pattern to what was observed on Figure 4.3a. The belonging of each case to its respective group has been assessed. Results indicate that 22 cases from cluster 2, 17 cases from cluster 3, 12 cases from cluster 4 and 9 cases from cluster 1 contributed to this pattern. In order to further elaborate on these differences, the evolution of the midlatitude flow for each cluster is presented and discussed in section 4.2.4.

4.2.4 Composite anomalies for different clusters

As in sections 4.1.4 and 4.1.5, time lagged composite anomalies for CH, PV and IVT after TC - jet interactions from cluster 1 are shown in this section. Figures 4 to 11 show results for clusters 2, 3 and 4 (cf. Appendices). On each panel, the 1st area investigated for precipitation extremes is represented by a dashed square and the adjusted area for the respective cluster is represented by a smaller solid rectangle.

Similarly to Figure 4.6, positive anomalies of condensational heating are observed along the eastern flank of the upstream trough on Figure 4.12a,b,c. These CH anomalies are again colocated with large positive IVT anomalies (Figure 4.13a,b,c). The initial flow situation on Figure 4.13a depicts the thin upstream trough mentioned in section 4.2.1 and a downstream ridge followed by a succession of weak PV anomalies, but no distinct trough. The 2PVU line from the analog flow situations (blue contour) exhibits a less-amplified upstream trough.

After 48 hours (Figure 4.13c), the trough-ridge couplet is slightly shifted to the east and remains well-amplified. A new trough begins to form downstream of the ridge. In comparison, the analog flow situation is actually becoming more zonal. Hence, positive (negative) PV anomalies co-located with the troughs (ridge) become more distinct; par-

ticularily, between 45 and 60° E, where the new trough is forming. During the next 48 hours, this new PV anomaly strengthens and remains located just to the west of the small solid rectangle. Positive IVT anomalies, oriented southwest-northeast, are indicative of

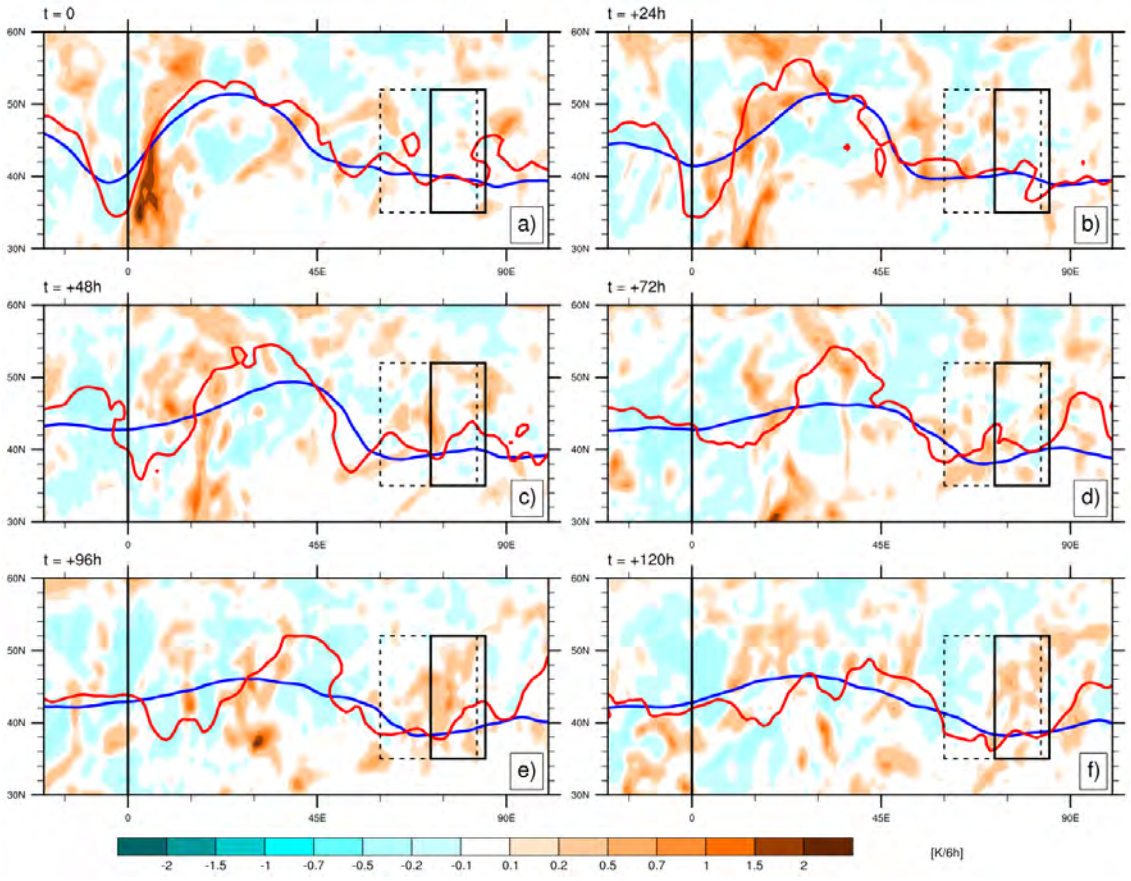

Figure 4.12: Condensational heating anomaly evolution for cluster 1 in [K/6h] (cyan-brown shadings). The red line represents the average isentropic 2PVU contour of the study cases. The blue line represents the average location of the 2PVU contour of the analog flow situations. Longitude 0 represents the location of the points of maximum interaction. The dotted black square represents the area where precipitation extremes are initially investigated and the smaller rectangle represents the redefined area for type - 1 interactions. Panel (a): composites at time 0. Panel (b): composites after 24 hours. Panel (c): composites after 48 hours. Panel (d) composites after 72 hours. Panel (e) composites after 96 hours. Panel (f) composites after 120 hours.

moisture transport into the rectangle. After 96 hours (Figure 4.13c), the red 2PVU contour exhibits a clear trough-ridge-trough pattern in comparison to the blue contour. The PV and IVT anomalies imply that TC - jet interactions from cluster 1 are conducive to an amplified flow with a downstream trough with an eastern flank located about 70° east from the point of maximum interaction. Positive IVT anomalies are located along this flank. Hence, a statistically significant increase in precipitation extremes is observed after 5 days between 72 and 85° E from the point of maximum interaction and 35 to 52°

N. A signature of these precipitation extremes is observed on Figure 4.12e,f as positive anomalies of condensational heating cover almost all the solid rectangle box. After 120 hours, the 2PVU line (red) exhibits a less amplified flow, which resembles more to the analog flow (blue). Positive IVT and CH anomalies are, however, still present over the box.

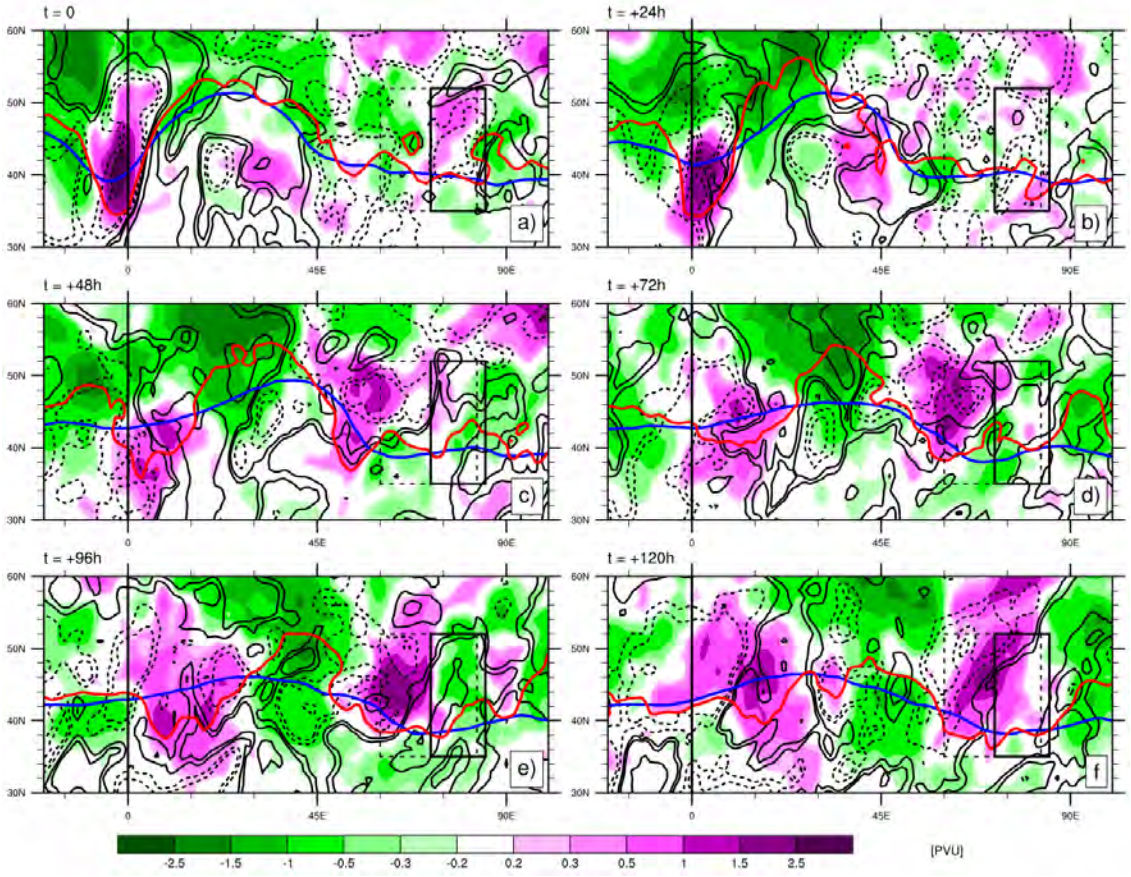

Figure 4.13: Potential vorticity and integrated vapor transport anomaly evolution for cluster 1. Purple (green) shadings indicated positive (negative) potential vorticity anomalies in [PVU]. Full (dotted) black contours represent positive (negative) IVT anomalies of -90, -30, -15, 15, 30 and 90 $[kg \cdot m^{-1} \cdot s^{-1}]$. The red line represents the average isentropic 2PVU contour of the study cases. The blue line represents the average location of the 2PVU contour of the analog flow situations. Longitude 0 represents the location of the points of maximum interaction. The dotted black square represents the area where precipitation extremes are initially investigated and the smaller rectangle represents the redefined area for type - 1 interactions. Panel (a): composites at time 0. Panel (b): composites after 24 hours. Panel (c): composites after 48 hours. Panel (d) composites after 72 hours. Panel (e) composites after 96 hours. Panel (f) composites after 120 hours.

For cluster 2, strong CH and IVT anomalies appear on the eastern flank of the upstream trough. 24 hours after TC - jet interaction (Fig. 4b), the downstream ridge amplifies (red line). In cases with no TC - jet interaction (blue line), the ridge does not amplify. After 48

hours, the strongest positive CH anomaly can be observed in the solid black rectangle (Fig. 4c). This positive anomaly occurs during the peak of precipitation extremes observed on Figure 3. At the same time, positive IVT anomalies are seen in the lower part of the rectangle, providing water for precipitation extremes (Fig. 5b,c). On panel (c), we can also observe a weak downstream trough, colocated with a positive anomaly, which could also contribute to the dynamic forcing for precipitation extremes. In the following 72 hours (panels d,e,f), the midlatitude flow's amplitude decreases and less CH and IVT anomalies can be observed in the downstream box.

Cluster 3 (Figures 7 and 8), exhibits a high amplitude initial flow at time 0. The blue line (analogs) from the analog composites describes correctly the general shape of the red line (study cases) but remains less amplified as in the other clusters. In this cluster, strong positive CH anomalies are observed at time 0 (Fig. 7a), but then, the anomalies decreases rapidly and are already much weaker 24 hours later (Fig. 7b). This cluster exhibits a rapid increase in precipitation extremes with a peak 48 hours after TC - jet interactions (cf. Fig. 6). We observe that just 24 hours after the interaction, a downstream trough associated with a positive PV anomaly is deepening (However, the PV anomaly was already present at time 0). The eastern flank of the trough is oriented southwest-northeast and located between 50 and 70° E from the point of maximum of interaction (Fig. 8b). Positive IVT anomalies from southwest to northeast along the eastern flank bring moist air into the area of interest. After 48 hours, the positive PV anomaly associated with the downstream trough is now extending from roughly 35° N - 45° E to 60° N - 75° E (Fig. 8c). The area of interest is located directly downstream of this anomaly and positive IVT anomalies are still directed towards it. On Figure 7b,c the precipitation extremes peak occurring at 48 hours (Fig. 6) is corroborated by positive anomalies of condensational heating in the box. After 72 hours, the amplitude of the 2PVU line (red line) reduces and CH, PV and IVT anomalies become weaker and less organized (Panels d, e and f). Therefore, precipitations extremes get closer to nominal values after the peak (cf. Fig. 6).

As for the other clusters, the signature of the tropical cyclones can be observed on Figure 10a in the CH positive anomalies downstream the reference longitude, for cluster 4. However, despite the diabatic processes occurring near the midlatitude waveguide, the evolution of the flow is very similar between cases from cluster 4 and the analogs (red and blue lines). No real amplification of the flow or development of a strong positive PV anomaly can be observed in the 5 days following the interactions. Figure 11a exhibits a long positive PV anomaly band east of the downstream ridge at time 0, but instead of reinforcing with time, it vanishes and becomes less organized. A few patches of positive CH anomalies can be observed on Figure 10c,d,e, in the dashed box. This indicates a slight increase of precipitation extremes between 48 and 96 hours as observed on Figures 12 and 13. However, the development of the atmospheric flow, after interactions from cluster 4, is not conducive to an increase of downstream precipitation extremes.

4.3 Discussion

4.3.1 Spatial scale of precipitation extremes

In section 4.2.3, we managed to define with more accuracy the location of the precipitation extremes after TC - jet interactions. The aim is to get the best approximation in terms of time and location to predict precipitation extremes after interactions of recurving tropical cyclones with the jet. However, due to the nature of the large scale processes in play and the variability within all cases, the signal in precipitation extremes increase is the strongest at a particular spatial scale. In other words, because of the variability between all cases, precipitation must be analyzed in a box, large enough to capture all events of precipitation extremes. But if the selected box is too large, we lose accuracy in the definition of the precipitation extremes' location. For TC - jet interactions from cluster 1, we obtain relative information about surface fraction and accumulated water in a 2.2 million squared-kilometers surface. If we reduce the size of the box, we might lose some information by not capturing some extremes happening outside of the box.

In the process of analyzing the different possibilities to assess precipitation extremes, we tried to assess the precipitation increase at the grid point level. By computing odds

ratio of getting precipitation extremes at each grid point individually, we realized that the signal was lost as we reduced the scale because of the variability between each case, even with similar initial flow situations. Therefore, the spatial information can only be as good as the consistence within all cases and the box size selection is crucial to capture the signal of precipitation extremes' increase.

4.3.2 Limits of the study

One major limit to this study arises from the large amount of processes and variables in play in TC - jet interactions and wave development. The initial visual analysis of 40 cases of recurving tropical cyclones has shown a large diversity of initial conditions and evolutions. Some cases showed downstream wave amplification with no or very little precipitation associated with elongated troughs. Other cases did not show any visible wave amplification. Sometimes, extratropical cyclones were already present in the Atlantic and interacted with the tropical cyclone. By isolating the effect of the jet stream configuration, we already managed to explain part of the variability in the downstream precipitation extremes response. However, each cluster still exhibited quite important variability. Considering the complexity of the reaction chain between the interaction onset and the precipitation extremes, parameters such as the strength of the interaction or the presence of warm conveyor belts should be included in the analysis to get a better understanding.

As mentioned, the second part of this study considered the flow situation at the moment of TC - jet interaction onsets as a key feature for the future development of precipitation extremes. Results from section 4.2.2 confirmed the different responses of precipitation extremes after different initial flow situations. In order to disentangle the effect of the recurving tropical cyclone from the natural evolution of the already wavy midlatitude waveguide, a novel technique has been used. Analog flow situations have been identified based on Euclidian distances of binary PV fields (see section 2.2.4). Although this technique is very promising, the selected analogues do not perfectly represent the geometry of the midlatitude flow during TC-jet interactions, especially for the upstream flow (cf. Figures 4.7 and 4.13). Since it was decided to keep the same intra-annual distribution of

events for the bootstrapping tests, analogs were only allowed to be picked in the same month as the real cases, thus limiting the amount of possible good candidates. This point is discussed in the outlook (Chapter 6).

Chapter 5

Conclusion

In this study, we addressed the question whether recurving tropical cyclones in the North Atlantic are conducive to precipitation extremes downstream. Previous studies have shown that the interaction between a recurving tropical cyclone and the jet stream leads to Rossby wave packet amplification. Following these findings, it has been suggested that recurving tropical cyclones could trigger downstream high impact weather events. Case studies have indeed established the link between some events of recurving TCs interacting with the jet and precipitation extremes. However, no study has provided a climatological evidence of the effect of recurving tropical cyclones on precipitation extremes.

Here we assessed the amount of downstream precipitation extremes after interactions between recurving North Atlantic TCs with the jet stream. Two metrics have been used to measure the amount of precipitation extremes. The first one measures the area affected by precipitation extremes. To this end, precipitation extremes in a downstream box were weighted with respect to their surface and summed up. The final product represents the fraction of the box covered by precipitation extremes. The second measure represents the precipitation volume exceeding the threshold used to define the extremes. For all grid points with precipitation extremes, the difference between the accumulated precipitation and the threshold used to define the extreme was computed and summed up in one column. In other words, this metric expresses the severity of the precipitation extremes.

We found that, on average, an area located between 60° and 83° E from the point of maximum interaction and 35° to 52° N records a doubling of the surface coverage be-

tween 30 and 72 hours after the TC - jet interaction onset compared the the climatology. Between 30 and 54 hours after TC - jet interaction, the precipitation extremes magnitude represents an accumulation of 50 mm/24h. This represents more than two times the climatology (i.e., 23.2 mm/24h). Quite large variability within the study sample has been found. A deeper analysis revealed that within the 147 cases, 41% did actually exhibit a similar increase pattern of precipitation extremes.

In the second part, we assessed the influence of the midlatitude flow configuration during the cyclone - jet interaction phase on the development of precipitation extremes. We applied a k-means clustering algorithm to PV fields around each point of interaction and defined 4 types of TC - jet interactions, based on the geometry of the jet stream. Individual assessments for each cluster revealed that on average, interaction cases from three clusters were followed by significantly more precipitation extremes than similar flow situations with no TC - jet interaction. Cluster 1 (21 cases) features a high latitude jet with a narrow upstream trough. TC - jet interactions are followed by a precipitation increase with a maximum after 120 hours. The precipitation extremes occur mainly in a box located 72 to 85° E from the points of maximum interaction and 35 to 52° N. Cluster 2 is the largest cluster with 54 cases. It features the most zonal flow of all clusters, with a low-amplitude upstream trough and a low-amplitude downstream ridge. It exhibits a precipitation extremes increase with a peak after 48 to 54 hours, between 60 and 69° E from the point of maximum interaction and 35° to 54° N. Cluster 3 (32 cases) features a well pre-amplified flow. This pre-amplified flow situation seems to be naturally conducive to precipitation extremes. However, cluster 3 exhibits a significant increase with an intense and short maximum after 48 hours. Interaction cases from clusters 4, featuring a similar but less amplified flow than cluster 3, did not show a significant increase in precipitation extremes.

The observed increase in precipitation extremes is explained by diabatic heating processes in the vicinity of the waveguide when the recurving TCs are approaching. It leads to a downstream wave packet amplification. An elongated upper-level trough can form and force air to ascend on its eastern flank. In the occurrence of sufficient moisture availability, significant amounts of water vapor can condensate and bring heavy precipitations.

Given the reduction of predictability of NWP (numerical weather prediction) models after interactions between recurving tropical cyclones and the midlatitude waveguide, these results might have possible applications for the improvement of weather forecasts after TC - jet interactions in the future. As mentioned in section 4.3.1, the area of prediction remains relatively coarse for the moment. But these promising results should motivate further investigation on the variability of the response to TC - jet interactions. The better we understand the different key parameters involved in the chain of processes, the better will the spatial and time prediction be. And thus, a real contribution to numerical weather predictions could be brought.

Chapter 6

Outlook

The results presented in the precedent chapter offer promising applications. In this section, future possible work is presented. This includes, possibilities of improvement of the method, further testing of the results and deeper understanding of the mechanisms leading to precipitation extremes.

- As mentioned in section 4.3.2, the analog flow situations had sometimes difficulties to accurately describe some important features of the real cases. This is partly due to a too small sample size but also to the detecting algorithm. There is therefore room for improvement of the algorithm for analog flow situations' detection. The latter could be improved by emphasizing the importance of the regions of interest that were poorly represented (i.e., the region located directly upstream of the point of maximum interaction). Hence, the binary fields used to measure Euclidian distance can be weighted with respect to the importance of the region. For instance, the region located directly upstream would hence, be multiplied by a factor which would immediately discriminate situations that do not exhibit very similar features in this zone. The aim is to get as close as possible to the real cases in order to isolate the effect of the recurving tropical cyclones.

- The method of maximum point interaction is a relevant method in this case to determine the location and time of the interaction onset. However, the strength of

this interaction has not been taken into account. Based on findings about Rossby wave amplification following TC - jet interaction, this parameter would be worth to be investigated to see if a linkage can be established between the strength of the interaction and the occurrence of precipitation extremes in addition to the current findings on flow types.

- This study concerns precipitation extremes following recurving North Atlantic tropical cyclones. However, extensive studies have been carried out in the Pacific and showed statistically significant Rossby wave amplification tropical cyclones' recurvature (*Archambault et al.*, 2013; *Quinting and Jones*, 2016). Hence, this method would also be applicable to other basins. Moreover, here we focused on precipitation extremes, but of high impact weather events, such as cold spells or heat waves could be attributed to a highly amplified jet following TC - jet interactions.

- Finally, a future and necessary step before any kind of application to NWP models can be imagined, would be to test the predictability of precipitation extremes following TC's recurvature. To this end, a precise metric that can be forecasted should be defined. The skill of the forecast could then be tested against a simple climatological baseline.

Appendices

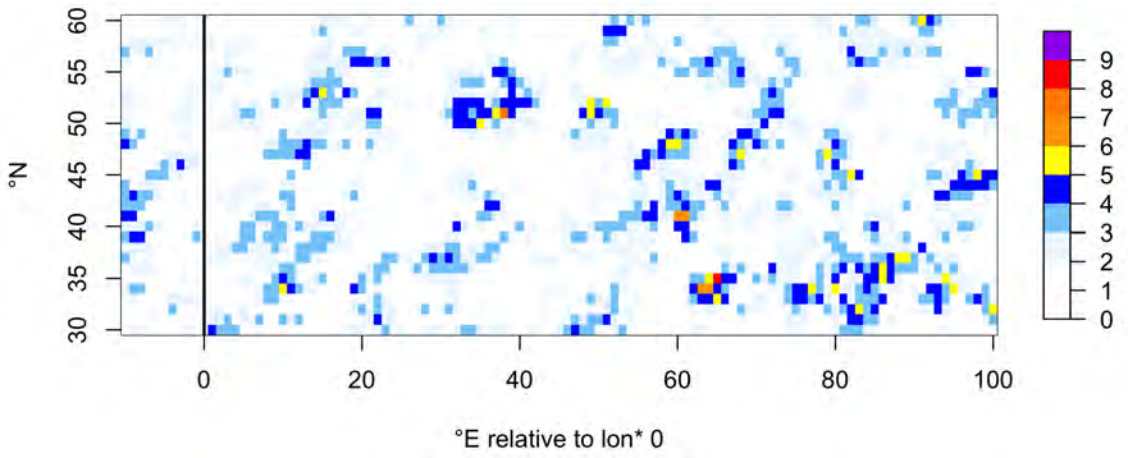

Figure 1: Precipitation extremes composite of 147 randomly picked days. The value at each grid point represents the number of precipitation extremes recorded in 147 random days. The vertical line represents the location where the points of maximum interaction happen for the cases of recurving tropical cyclones.

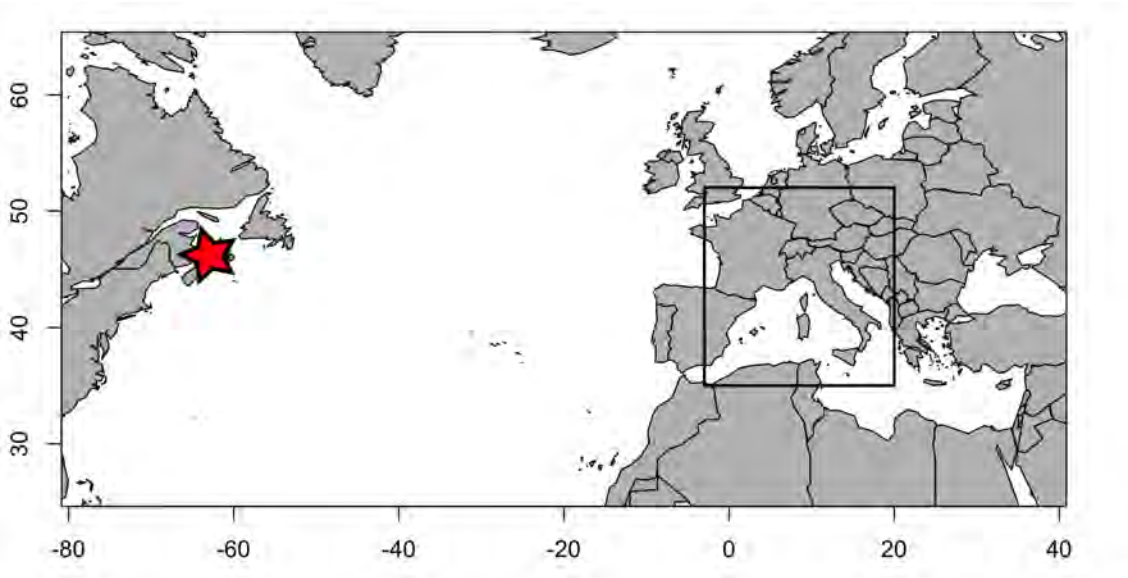

Figure 2: Projection of the area investigated for precipitation extremes based on the average location of the maximum interaction points. The star represents the average location of the maximum interaction points (63° W and 46° N). The box is located between 3° W and 20° E and 35 to 52° N.

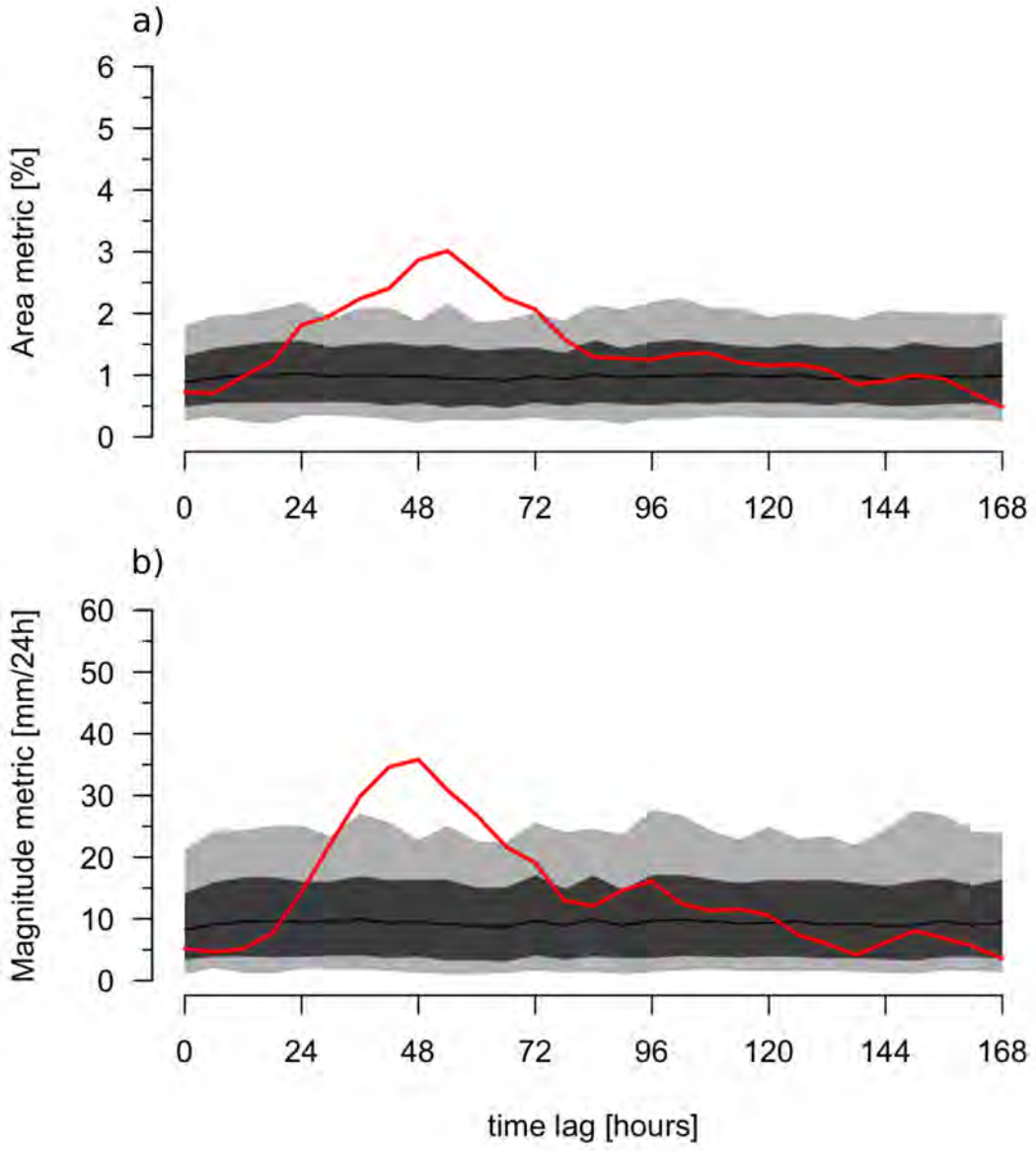

Figure 3: Time series of precipitation extremes for cluster 2 in a redefined grid box. Panel (a): The vertical axis represents the fraction in [%] of the new grid box recording precipitation extremes at a given time after the interaction. Panel (b): The vertical axis represents the magnitude metric in [mm/24h] in the new grid box. The red line represents the average of 54 recurving TC events. The light and dark gray shadings respectively represent the empirical 1^{st}-99^{th} and the 10^{th}-90^{th} intervals of precipitation extremes obtained from the bootstrapping test. The black line represents the mean of the bootstrapping distribution.

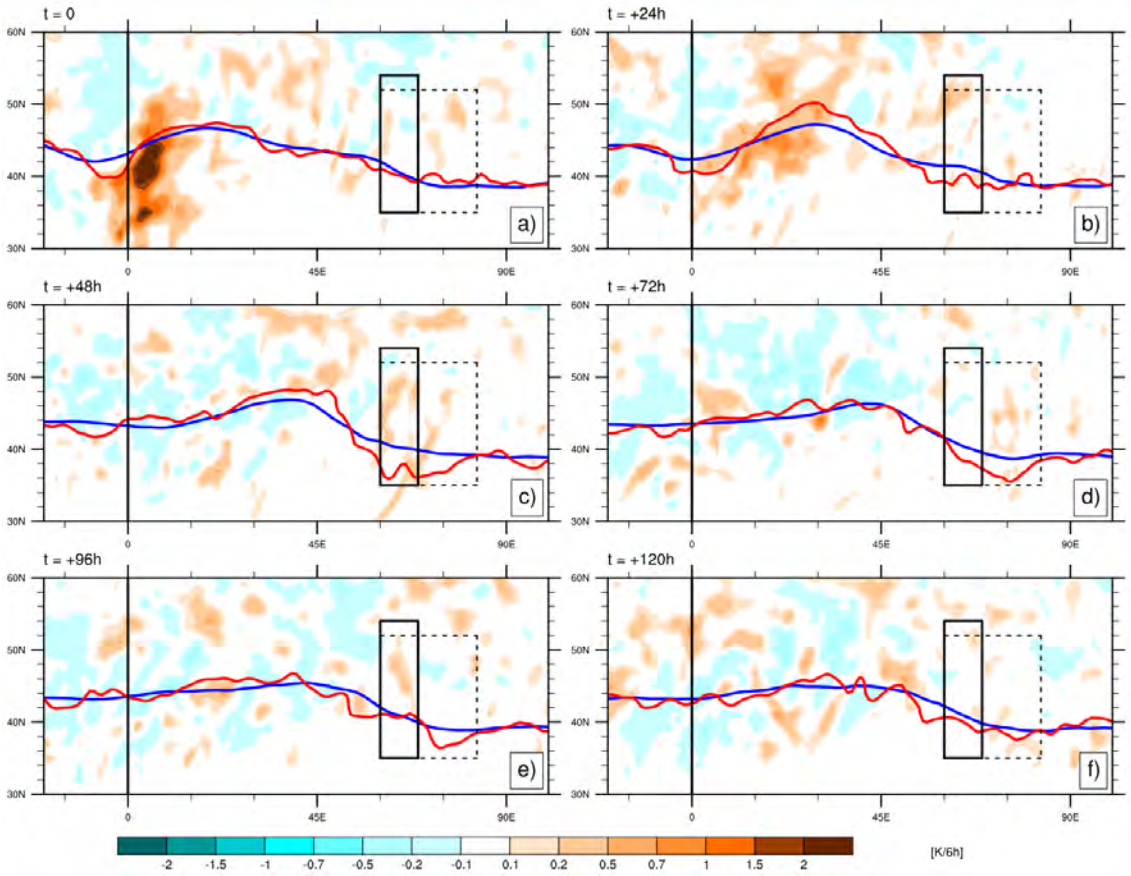

Figure 4: Condensational heating anomaly evolution for cluster 2 in [K/6h] (cyan-brown shadings). The red line represents the average isentropic 2PVU contour of the study cases. The blue line represents the average location of the 2PVU contour of the analog flow situations. Longitude 0 represents the location of the points of maximum interaction. The dotted black square represents the area where precipitation extremes are initially investigated and the smaller rectangle represents the redefined area for type - 2 interactions. Panel (a): composites at time 0. Panel (b): composites after 24 hours. Panel (c): composites after 48 hours. Panel (d) composites after 72 hours. Panel (e) composites after 96 hours. Panel (f) composites after 120 hours.

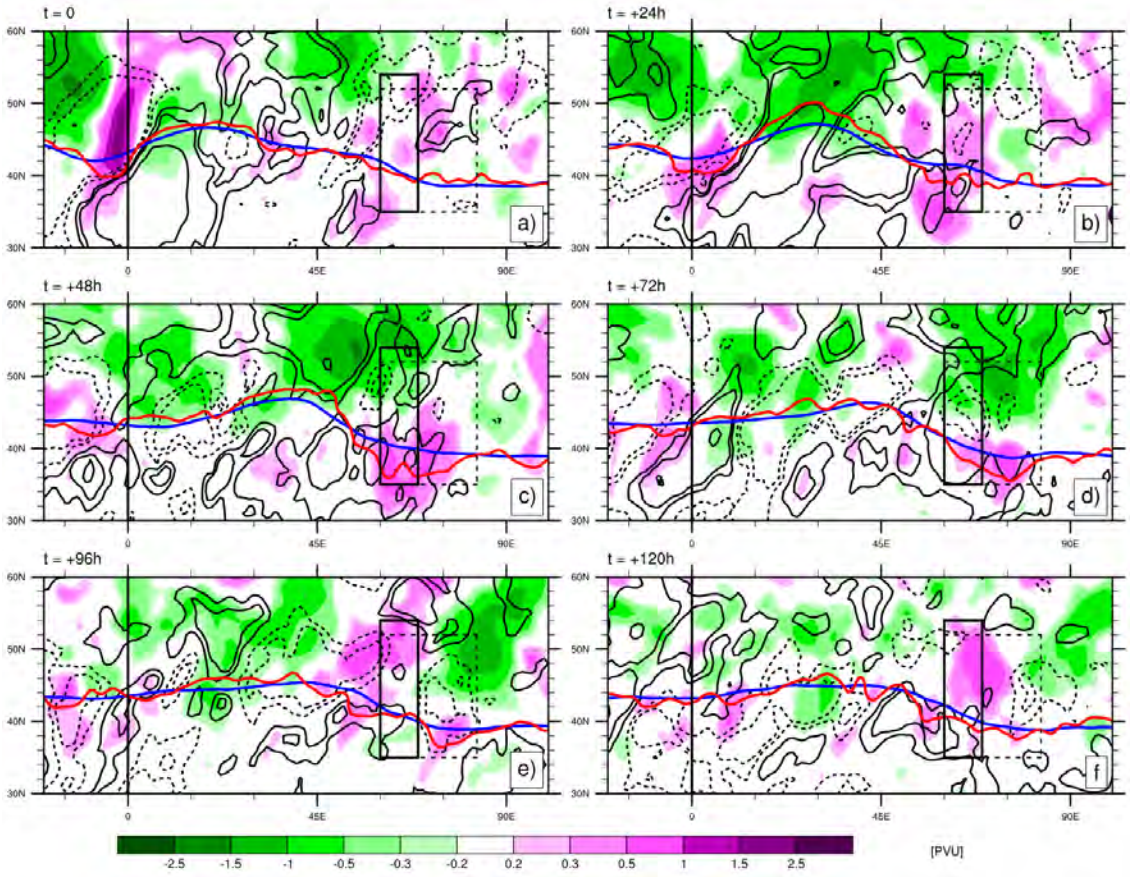

Figure 5: Potential vorticity and integrated vapor transport anomaly evolution for cluster 2. Purple (green) shadings indicated positive (negative) potential vorticity anomalies in [PVU]. Full (dotted) black contours represent positive (negative) IVT anomalies of -90, -30, -15, 15, 30 and 90 $[kg \cdot m^{-1} \cdot s^{-1}]$. The red line represents the average isentropic 2PVU contour of the study cases. The blue line represents the average location of the 2PVU contour of the analog flow situations. Longitude 0 represents the location of the points of maximum interaction. The dotted black square represents the area where precipitation extremes are initially investigated and the smaller rectangle represents the redefined area for type - 2 interactions. Panel (a): composites at time 0. Panel (b): composites after 24 hours. Panel (c): composites after 48 hours. Panel (d) composites after 72 hours. Panel (e) composites after 96 hours. Panel (f) composites after 120 hours.

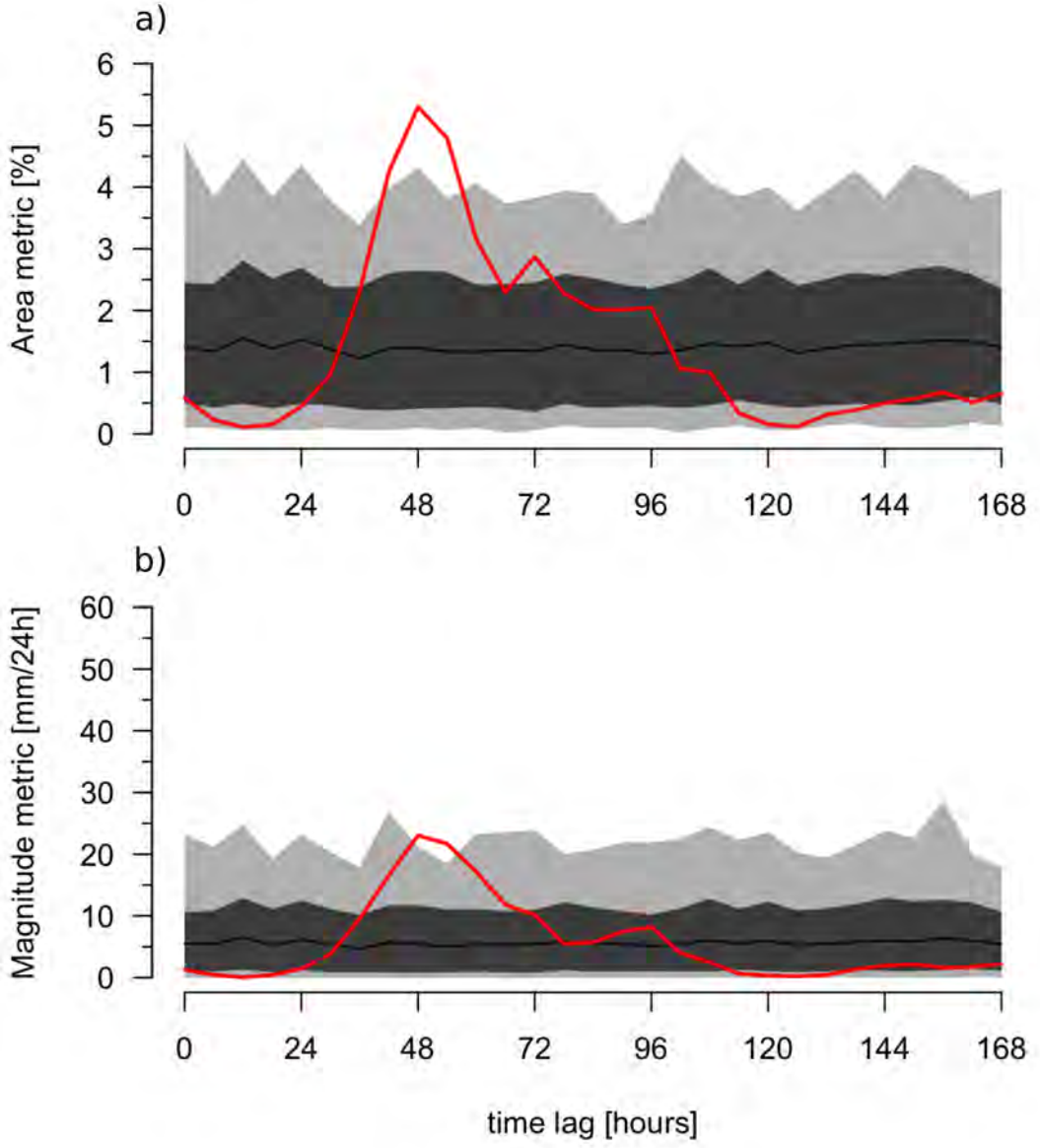

Figure 6: Time series of precipitation extremes for cluster 3 in a redefined grid box. Panel (a): The vertical axis represents the fraction in [%] of the new grid box recording precipitation extremes at a given time after the interaction. Panel (b): The vertical axis represents the magnitude metric in [mm/24h] in the new grid box. The red line represents the average of 32 recurving TC events. The light and dark gray shadings respectively represent the empirical 1^{st}-99^{th} and the 10^{th}-90^{th} intervals of precipitation extremes obtained from the bootstrapping test. The black line represents the mean of the bootstrapping distribution.

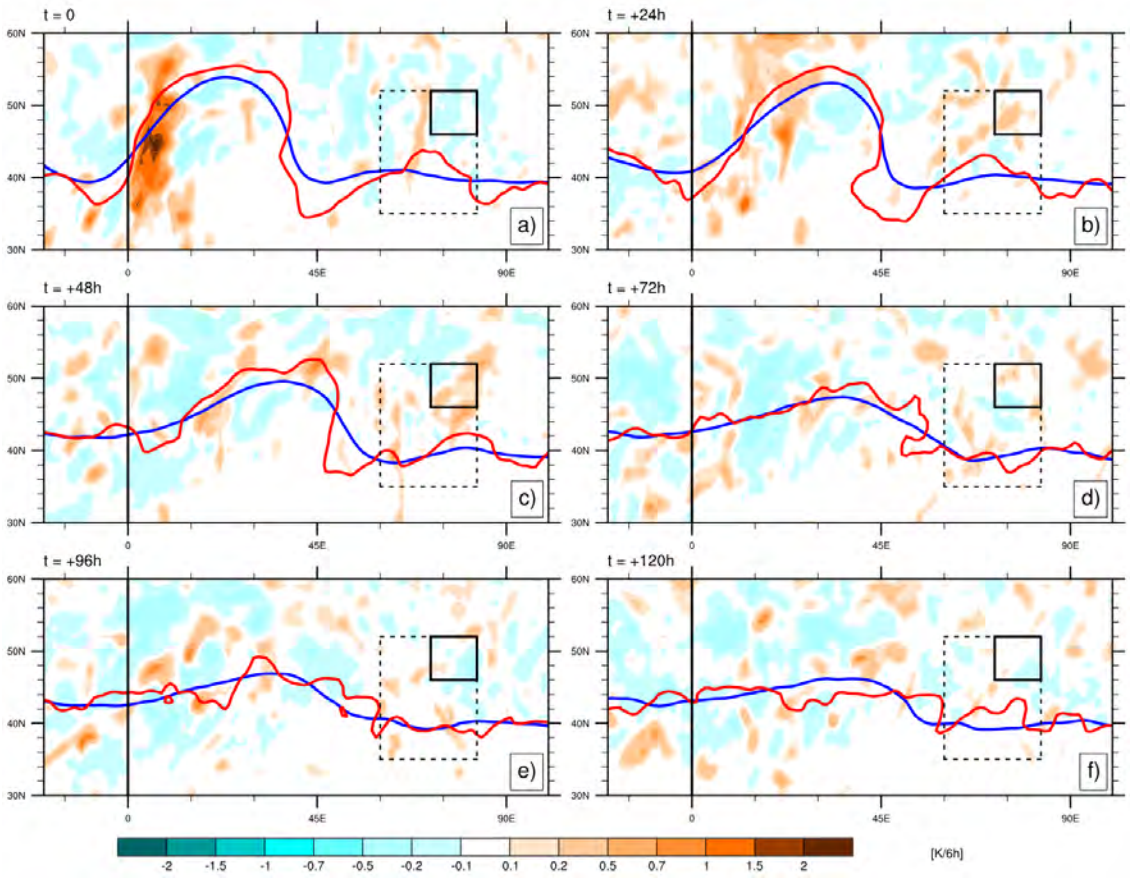

Figure 7: Condensational heating anomaly evolution after interactions from cluster 3 in [K/6h] (cyan-brown shadings). The red line represents the average isentropic 2PVU contour of the study cases. The blue line represents the average location of the 2PVU contour of the analog flow situations. Longitude 0 represents the location of the points of maximum interaction. The dotted black square represents the area where precipitation extremes are initially investigated and the smaller rectangle represents the redefined area for type - 3 interactions. Panel (a): composites at time 0. Panel (b): composites after 24 hours. Panel (c): composites after 48 hours. Panel (d) composites after 72 hours. Panel (e) composites after 96 hours. Panel (f) composites after 120 hours.

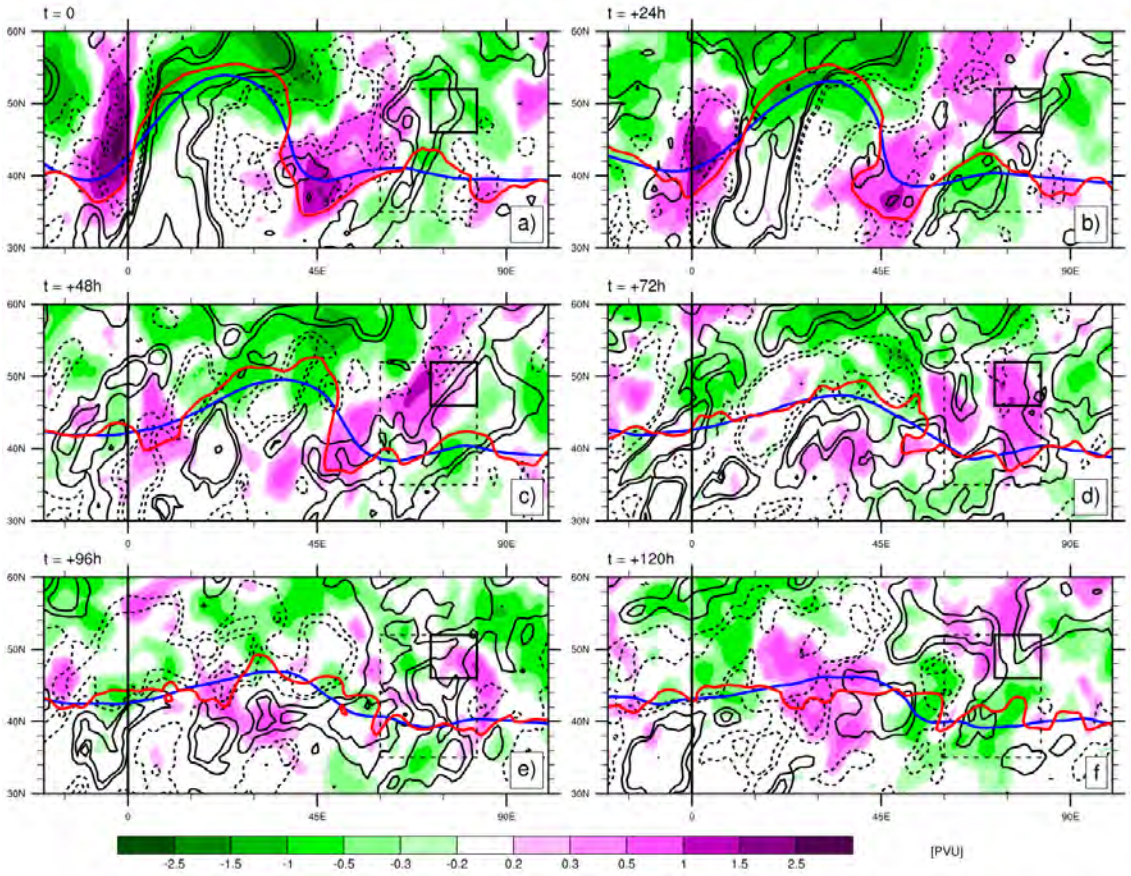

Figure 8: Potential vorticity and integrated vapor transport anomaly for cluster 3. Purple (green) shadings indicated positive (negative) potential vorticity anomalies in [PVU]. Full (dotted) black contours represent positive (negative) IVT anomalies of -90, -30, -15, 15, 30 and 90 $[kg \cdot m^{-1} \cdot s^{-1}]$. The red line represents the average isentropic 2PVU contour of the study cases. The blue line represents the average location of the 2PVU contour of the analog flow situations. Longitude 0 represents the location of the points of maximum interaction. The dotted black square represents the area where precipitation extremes are initially investigated and the smaller rectangle represents the redefined area for type - 3 interactions. Panel (a): composites at time 0. Panel (b): composites after 24 hours. Panel (c): composites after 48 hours. Panel (d) composites after 72 hours. Panel (e) composites after 96 hours. Panel (f) composites after 120 hours.

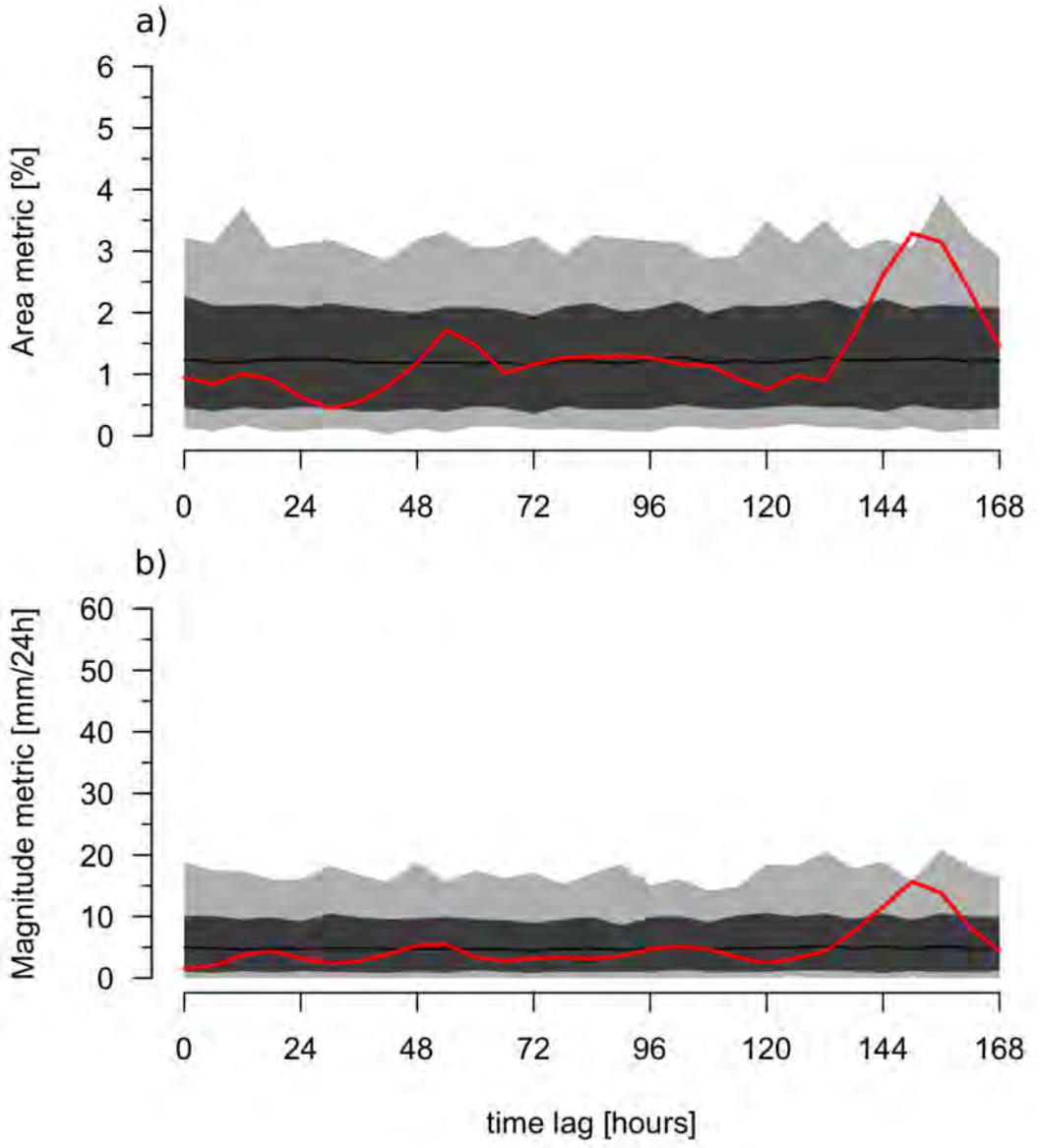

Figure 9: Time series of precipitation extremesfor cluster 4 in a redefined grid box. Panel (a): The vertical axis represents the fraction in [%] of the new grid box recording precipitation extremes at a given time after the interaction. Panel (b): The vertical axis represents the magnitude metric in [mm/24h] in the new grid box. The red line represents the average of 40 recurving TC events. The light and dark gray shadings respectively represent the empirical 1^{st}-99^{th} and the 10^{th}-90^{th} intervals of precipitation extremes obtained from the bootstrapping test. The black line represents the mean of the bootstrapping distribution.

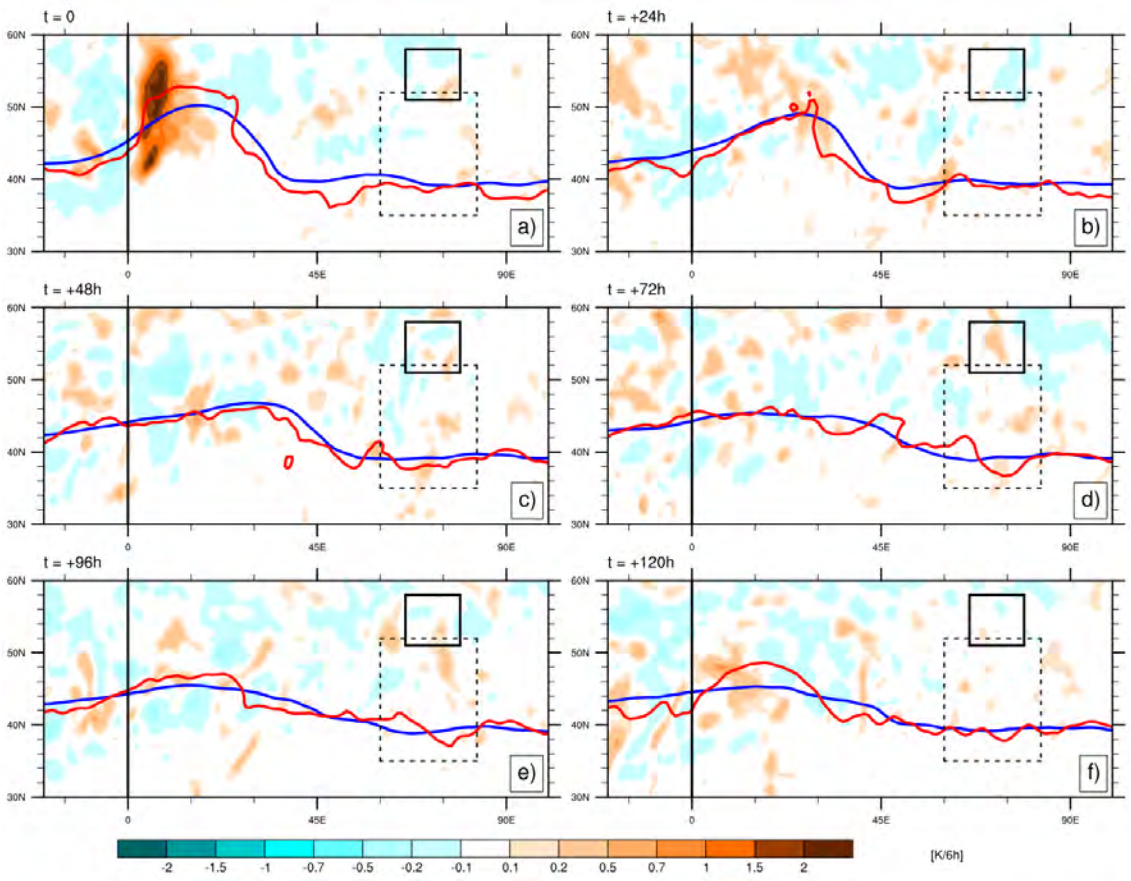

Figure 10: Condensational heating anomaly evolution for cluster 4 in [K/6h] (cyan-brown shadings). The red line represents the average isentropic 2PVU contour of the study cases. The blue line represents the average location of the 2PVU contour of the analog flow situations. Longitude 0 represents the location of the points of maximum interaction. The dotted black square represents the area where precipitation extremes are initially investigated and the smaller rectangle represents the redefined area for type - 4 interactions. Panel (a): composites at time 0. Panel (b): composites after 24 hours. Panel (c): composites after 48 hours. Panel (d) composites after 72 hours. Panel (e) composites after 96 hours. Panel (f) composites after 120 hours.

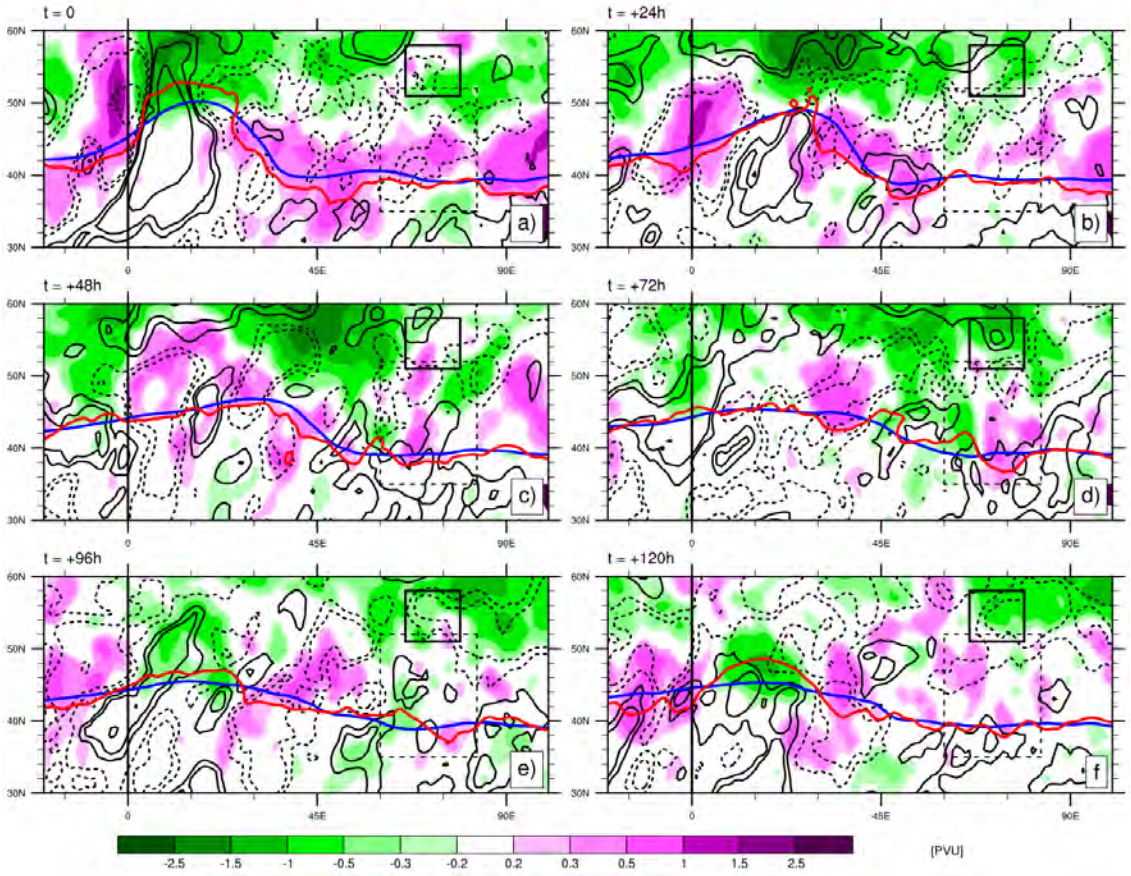

Figure 11: Potential vorticity and integrated vapor transport anomaly evolution for cluster 4. Purple (green) shadings indicated positive (negative) potential vorticity anomalies in [PVU]. Full (dotted) black contours represent positive (negative) IVT anomalies of -90, -30, -15, 15, 30 and 90 $[kg \cdot m^{-1} \cdot s^{-1}]$. The red line represents the average isentropic 2PVU contour of the study cases. The blue line represents the average location of the 2PVU contour of the analog flow situations. Longitude 0 represents the location of the points of maximum interaction. The dotted black square represents the area where precipitation extremes are initially investigated and the smaller rectangle represents the redefined area for type - 4 interactions. Panel (a): composites at time 0. Panel (b): composites after 24 hours. Panel (c): composites after 48 hours. Panel (d) composites after 72 hours. Panel (e) composites after 96 hours. Panel (f) composites after 120 hours.

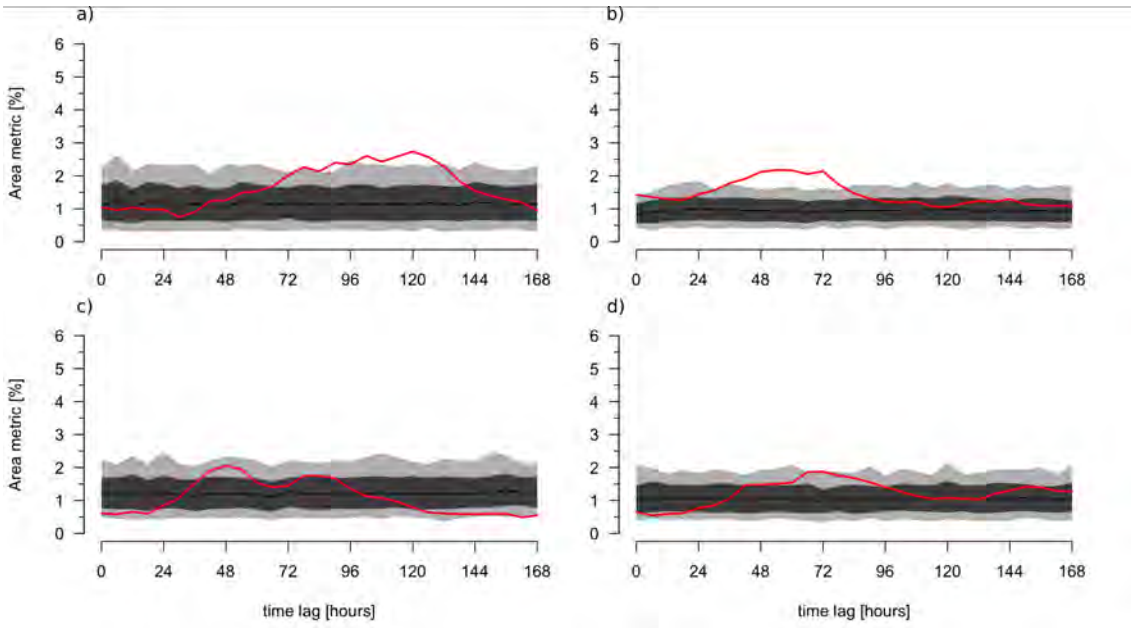

Figure 12: Time series of precipitation extremes after TC - jet interactions for each cluster. The horizontal axis represents the time lag after TC - jet interaction onsets. The vertical axis represents the fraction in [%] of the grid box covered by precipitation extremes at a given lag after the interaction. The red line represents the average of recurving TC events of the respective group. The light and dark gray shadings respectively represent the empirical 1^{st}-99^{th} and the 10^{th}-90^{th} intervals of precipitation extremes obtained from the bootstrapping test. The black line represents the mean of the bootstrapping distribution. Panel (a): Cluster 1 Panel (b): Cluster 2 Panel (c): Cluster 3 Panel (d): Cluster 4

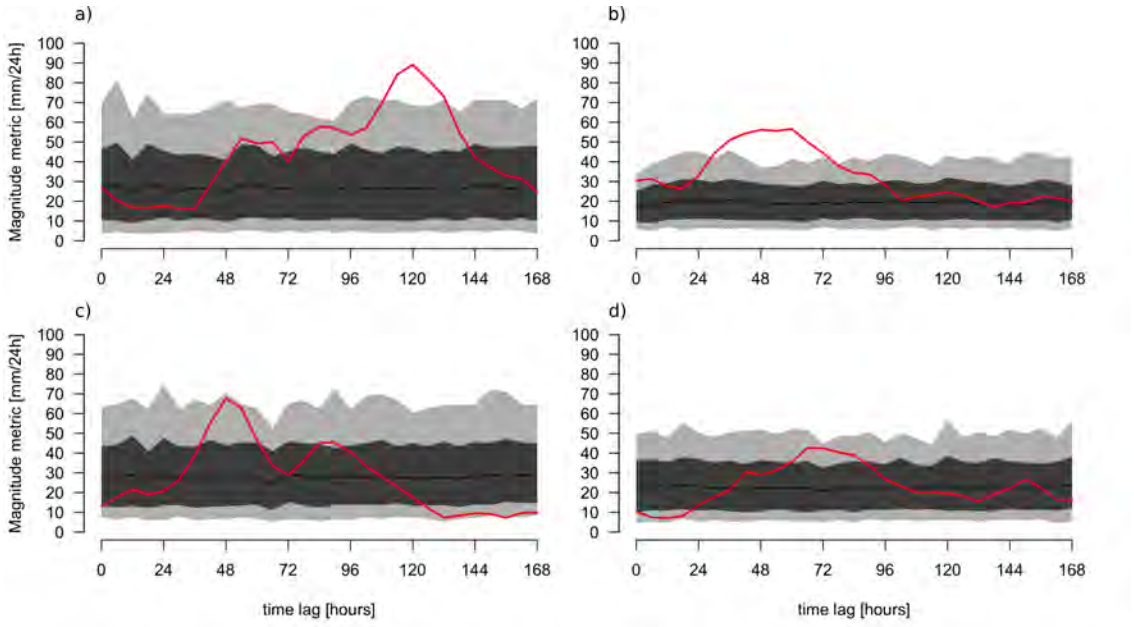

Figure 13: Same as figure 12, but the vertical axis represents the magnitude metric in [mm/24h] in the grid box.

Figures 12 and 13 show the results of the precipitation extremes evolution after TC - jet interactions for the 4 different clusters in the initial box (60 - 82° E from point of maximum interaction and 35 to 52° N), for a more direct comparison between all clusters. The evolutions and magnitudes of precipitation extremes differ for each cluster. Thus, cases from clusters 2, 3 and 4 (126 cases in total) are contributing more to the general tendency with a peak in precipitation extremes at 48 hours (Figure 4.3) than cases from cluster 1, as seen in Section 4.2.2. However, on average clusters 3 and 4 do not show statistically significant increases compared to their respective bootstrapping test (Figures 12c,d and 13c,d) The mean precipitation extremes time series remains within the 1^{st}-99^{th} quantile range.

On the other hand, clusters 1 and 2 show an increase in both metrics (Figures 12 and 13, panels (a) and (b)) exceeding the empirical 99^{th} percentile. Cluster 2 exhibits a plateau of precipitation extremes surface coverage between +48 and +72 hours with values up to 2.14% of the grid box (Figure 12b). The mean values obtained from the bootstrapping oscillate between 0.88 and 0.94% during these time lags. Therefore, more than a doubling of the surface covered by precipitation extremes is observed after TC - jet interactions compared to the analogue situations. In terms of precipitation extremes magnitude, the signal is even stronger and reaches a fourfold increase compared to the mean of the bootstrapping distribution. Cluster 2 is perhaps the most interesting case as it represents the most zonal initial flow and the largest cluster. The precipitation extremes increase is therefore conceivably the result of an amplification of the flow following the TC interaction. Compared to clusters 2, 3 and 4, cluster 1 exhibits a much later peak in both metrics. The maximum values are obtained at +120 hours with respective values of 2.73% and 89.2 mm/24h. Hence, between 96 and 120 hours after a type 1 TC - jet interaction (cases from cluster 1), a 2.7 times larger area is covered by precipitation extremes and the magnitude metric is multiplied by 3.7.

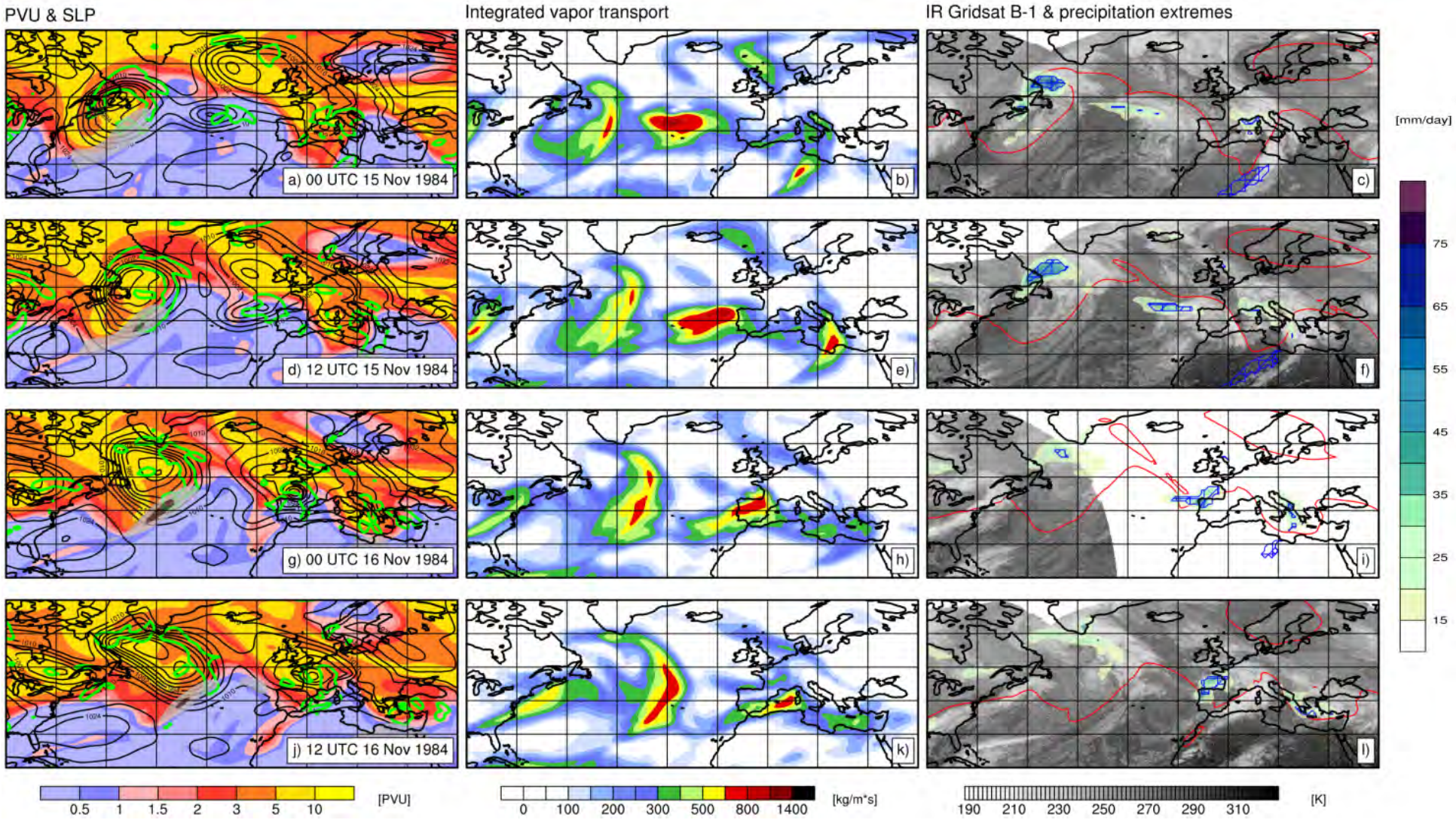

Figure 14: Hurricane Klaus' overview: Panels (a-d-g-j): potential vorticity at the 335 K isentropic surface in [PVU] (1 PVU = $10^{-6} \cdot K \cdot m^2 \cdot s^{-1} \cdot kg^{-1}$), horizontal wind at 335K above 55, 65 and 75 [m/s] (grey shadings) and ascending air at 500 [hPa] larger than -0.3 [hPa/s] (green contours). Panels (b-e-h-k): Integrated vapor transport in $[kg \cdot m^{-1} \cdot s^{-1}]$. Panels (c-f-i-l): IR satellite images of brightness temperature near 11 microns in [K], daily accumulated precipitation [mm/24h] and precipitation extremes (blue hatches).

Bibliography

Agusti-Panareda, A., C. Thorncroft, G. Craig, and S. Gray (2004), The extratropical transition of Hurricane Irene (1999): A potential-vorticity perspective, *Quarterly Journal of the Royal Meteorological Society*, *130*(598), 1047–1074, doi:10.1256/qj.02.140.

Anwender, D., P. A. Harr, and S. C. Jones (2008), Predictability associated with the downstream impacts of the extratropical transition of tropical cyclones: Case studies, *Monthly Weather Review*, *136*(9), 3226–3247, doi:10.1175/2008MWR2249.1.

Archambault, H. M., L. F. Bosart, D. Keyser, and J. M. Cordeira (2013), A climatological analysis of the extratropical flow response to recurving western North Pacific tropical cyclones, *Monthly Weather Review*, *141*(7), 2325–2346, doi:10.1175/MWR-D-12-00257.1.

Cordeira, J. M., and L. F. Bosart (2011), Cyclone interactions and evolutions during the "Perfect Storms" of late October and early November 1991, *Monthly Weather Review*, *139*(6), 1683–1707.

Dee, D., S. M. Uppala, and F. Vitart (2011), The ERA-Interim reanalysis: configuration and performance of the data assimilation system, *Quarterly Journal of the Royal Meteorological Society*, *137*, 553–597, doi:10.1002/qj.828.

Emanuel, K. (2003), TROPICAL CYCLONES, *Annual Review of Earth and Planetary Sciences*, *31*(1), 75–104, doi:10.1146/annurev.earth.31.100901.141259.

Grams, C. M., and H. M. Archambault (2016), The key role of diabatic outflow in amplifying the midlatitude flow: A representative case study of weather systems surround-

ing western North Pacific extratropical transition, *Monthly Weather Review*, *144*(10), 3847–3869, doi:10.1175/MWR-D-15-0419.1.

Grams, C. M., and S. R. Blumer (2015), European high-impact weather caused by the downstream response to the extratropical transition of North Atlantic Hurricane Katia (2011), *Geophysical Research Letters*, *42*(20), 8738–8748, doi:10.1002/2015GL066253.

Grams, C. M., H. Wernli, M. Böttcher, J. Čampa, U. Corsmeier, S. C. Jones, J. H. Keller, C.-J. Lenz, and L. Wiegand (2011), The key role of diabatic processes in modifying the upper-tropospheric wave guide: a North Atlantic case-study, *Quarterly Journal of the Royal Meteorological Society*, *137*(661), 2174–2193, doi:10.1002/qj.891.

Grams, C. M., S. T. Lang, and J. H. Keller (2015), A quantitative assessment of the sensitivity of the downstream midlatitude flow response to extratropical transition of tropical cyclones, *Geophysical Research Letters*, *42*(21), 9521–9529, doi:10.1002/2015GL065764.

Grazzini, F., and F. Vitart (2015), Atmospheric predictability and Rossby wave packets, *Quarterly Journal of the Royal Meteorological Society*, *141*(692), 2793–2802, doi:10.1002/qj.2564.

Hakim, G. J. (2003), Developing wave packets in the North Pacific storm track, *Monthly Weather Review*, *131*(11), 2824–2837, doi:10.1175/1520-0493(2003)131⟨2824:DWPITN⟩2.0.CO;2.

Hanley, D., J. Molinari, and D. Keyser (2001), A composite study of the interactions between tropical cyclones and upper-tropospheric troughs, *Monthly Weather Review*, *129*(10), 2570–2584, doi:10.1175/1520-0493.

Harr, P. A., and J. M. Dea (2009), Downstream development associated with the extratropical transition of tropical cyclones over the western North Pacific, *Monthly Weather Review*, *137*(4), 1295–1319, doi:10.1175/2008MWR2558.1.

Hart, R. E., and J. L. Evans (2001), A climatology of the extratropical transition of Atlantic tropical cyclones, *Journal of Climate*, *14*(4), 546–564, doi:10.1175/1520-0442.

Hart, R. E., and J. L. Evans (2003), A cyclone phase space derived from thermal wind and thermal asymmetry, *Monthly Weather Review*, *131*(4), 585–616, doi:10.1175/1520-0493.

Hoskins, B. J., M. McIntyre, and A. W. Robertson (1985), On the use and significance of isentropic potential vorticity maps, *Quarterly Journal of the Royal Meteorological Society*, *111*(470), 877–946, doi:10.1002/qj.49711147002.

Jones, S. C., P. A. Harr, J. Abraham, L. F. Bosart, P. J. Bowyer, J. L. Evans, D. E. Hanley, B. N. Hanstrum, R. E. Hart, F. Lalaurette, et al. (2003), The extratropical transition of tropical cyclones: Forecast challenges, current understanding, and future directions, *Weather and Forecasting*, *18*(6), 1052–1092, doi:10.1175/1520-0434.

Klein, P. M., P. A. Harr, and R. L. Elsberry (2000), Extratropical transition of western North Pacific tropical cyclones: An overview and conceptual model of the transformation stage, *Weather and Forecasting*, *15*(4), 373–395, doi:10.1175/1520-0434.

Knapp, K. R., M. C. Kruk, D. H. Levinson, H. J. Diamond, and C. J. Neumann (2010), The international best track archive for climate stewardship (IBTrACS), *Bulletin of the American Meteorological Society*, *91*(3), 363, doi:10.1175/2009BAMS2755.1.

Knapp, K. R., S. Ansari, C. L. Bain, M. A. Bourassa, M. J. Dickinson, C. Funk, C. N. Helms, C. C. Hennon, C. D. Holmes, G. J. Huffman, et al. (2011), Globally gridded satellite observations for climate studies, *Bulletin of the American Meteorological Society*, *92*(7), 893–907, doi:10.1175/2011BAMS3039.1.

Kofron, D. E., E. A. Ritchie, and J. S. Tyo (2010), Determination of a consistent time for the extratropical transition of tropical cyclones. Part i: Examination of existing methods for finding "ET time", *Monthly Weather Review*, *138*(12), 4328–4343, doi:10.1175/2010MWR3180.1.

Lawrence, M. B., and G. B. Clark (1985), ANNUAL SUMMARY Atlantic Hurricane Season of 1984, *Monthly Weather Review*.

Martius, O., E. Zenklusen, C. Schwierz, and H. C. Davies (2006), Episodes of Alpine heavy precipitation with an overlying elongated stratospheric intrusion: A climatology, *International Journal of Climatology*, *26*(9), 1149–1164, doi:10.1002/joc.1295.

Martius, O., C. Schwierz, and H. Davies (2008), Far-upstream precursors of heavy precipitation events on the Alpine south-side, *Quarterly Journal of the Royal Meteorological Society*, *134*(631), 417–428, doi:10.1002/qj.229.

Massacand, A. C., H. Wernli, and H. C. Davies (2001), Influence of upstream diabatic heating upon an Alpine event of heavy precipitation, *Monthly Weather Review*, *129*(11), 2822–2828, doi:10.1175/1520-0493.

Orlanski, I., and J. P. Sheldon (1995), Stages in the energetics of baroclinic systems, *Tellus A*, *47*(5), 605–628, doi:10.1034/j.1600-0870.1995.00108.x.

Pantillon, F., J.-P. Chaboureau, and E. Richard (2015), Remote impact of North Atlantic hurricanes on the Mediterranean during episodes of intense rainfall in autumn 2012, *Quarterly Journal of the Royal Meteorological Society*, *141*(688), 967–978, doi:10.1002/qj.2419.

Pantillon, F. P., J.-P. Chaboureau, P. J. Mascart, and C. Lac (2013), Predictability of a Mediterranean tropical-like storm downstream of the extratropical transition of Hurricane Helene (2006), *Monthly Weather Review*, *141*(6), 1943–1962, doi:10.1175/MWR-D-12-00164.1.

Pasch, R. J., E. S. Blake, H. D. Cobb III, and D. P. Roberts (2006), Tropical Cyclone Report: Hurricane Wilma (AL252005) 15-25 october 2005, *Technical Report, National Hurricane Center*.

Pinto, J., M. Klawa, U. Ulbrich, R. Rudari, and P. Speth (2001), Extreme precipitation events over northwest Italy and their relationship with tropical–extratropical interactions over the Atlantic, in *Proceedings of the third EGS Plinius Conference on Mediterranean Storms, Baja Sardinia, Italy, GNDCI Publication*, 2560, pp. 321–332.

Quinting, J. F., and S. C. Jones (2016), On the impact of tropical cyclones on rossby wave packets: A climatological perspective, *Monthly Weather Review*, *144*(5), 2021–2048, doi:10.1175/MWR-D-14-00298.1.

Riemer, M., and S. C. Jones (2010), The downstream impact of tropical cyclones on a

developing baroclinic wave in idealized scenarios of extratropical transition, *Quarterly Journal of the Royal Meteorological Society*, *136*(648), 617–637, doi:10.1002/qj.605.

Riemer, M., S. C. Jones, and C. A. Davis (2008), The impact of extratropical transition on the downstream flow: An idealized modelling study with a straight jet, *Quarterly Journal of the Royal Meteorological Society*, *134*(630), 69–92, doi:10.1002/qj.189.

Ritchie, E. A., and R. L. Elsberry (2007), Simulations of the extratropical transition of tropical cyclones: Phasing between the upper-level trough and tropical cyclones, *Monthly Weather Review*, *135*(3), 862–876, doi:10.1175/MWR3303.1.

Röthlisberger, M., S. Pfahl, and O. Martius (2016), Regional-scale jet waviness modulates the occurrence of mid-latitude weather extremes, *Geophysical Research Letters*, doi:10.1002/2016GL070944.

Stewart, S. R. (2013), Tropical Cyclone Report: Hurricane Leslie (AL122012) 30 august – 11 september 2012, *Technical Repport, National Hurricane Center*.

Studholme, J., K. I. Hodges, and C. M. Brierley (2015), Objective determination of the extratropical transition of tropical cyclones in the Northern Hemisphere, *Tellus A: Dynamic Meteorology and Oceanography*, *67*(1), 24,474, doi:10.3402/tellusa.v67.24474.

Teubler, F., and M. Riemer (2016), Dynamics of rossby wave packets in a quantitative potential vorticity–potential temperature framework, *Dynamics*, doi:10.1175/JAS-D-15-0162.1.

Wernli, B. H., and H. C. Davies (1997), A Lagrangian-based analysis of extratropical cyclones. i: The method and some applications, *Quarterly Journal of the Royal Meteorological Society*, *123*(538), 467–489, doi:10.1002/qj.49712353811.

Yuen, K. K. (1974), The two-sample trimmed t for unequal population variances, *Biometrika*, *61*(1), 165–170, doi:10.1093/biomet/61.1.165.

List of Figures

Acknowledgements

First of all, I would like to thank my supervisor, Olivia Martius-Romppainen, for her support during this Master Thesis. I am very grateful for her precious advices and the time she took to supervise my work. Moreover, I am very grateful for the trust she put in me when proposing this very interesting topic and for letting me carry out this research with much freedom. It has been a great experience to work in this environment, surrounded by very competent people, always keen to help whenever needed. Therefore, I would like to thank Sina Lenggenhager, Yannick Barton, Luca Panziera and Andrey Martinov for their availability and much needed assistance.

I also would like to mention Christian Grams and Jacopo Riboldi from ETHZ, whose involvement in my project was a real motivation for me. I would like to thank them for their interest, time and precious guidance and moreover, for the precious dataset on PV advection and review provided by Jacopo.

Finally, I need to address a big thank you to Matthias Röthlisberger who has been there for me and assisted me throughout this project. Thank you for all the time you spent on my work, for you numerous advices, the precious scripts and for the Hoskin's paper reading sessions.

To all these people: Thank you very much!

Declaration

under Art. 28 Para. 2 RSL 05

Last, first name:	Pohorsky, Roman
Matriculation number:	09-406-778
Programme:	Climate Sciences Bachelor ☐ Master ☒ Dissertation ☐
Thesis title:	A climatological analysis of downstream precipitation extremes associated with recurving North Atlantic tropical cyclones
Thesis supervisor:	Prof. Dr. Olivia Romppainen-Martius

I hereby declare that this submission is my own work and that, to the best of my knowledge and belief, it contains no material previously published or written by another person, except where due acknowledgement has been made in the text. In accordance with academic rules and ethical conduct, I have fully cited and referenced all material and results that are not original to this work. I am well aware of the fact that, on the basis of Article 36 Paragraph 1 Letter o of the University Law of 5 September 1996, the Senate is entitled to deny the title awarded on the basis of this work if proven otherwise. I grant inspection of my thesis.

Bern, 08.09.2017

Signature